

Characterization of the degradation behaviour of Passive Fire Protector Materials

Dipartimento di Ingegneria Chimica, Mineraria e Delle Tecnologie Ambientali

Via Terracini, 34 - 40131 Bologna

Alma Mater Studiorum – Università di Bologna

Student: Celia Anaut Rufas

Tutor: Prof. Valerio Cozzani

Supervisors: Alessandro Tugnoli

Mercedes Gómez Mares

February 2011

Acknowledgements

I would like to thank all the people who made this thesis possible.

First, I would like to thank Professoressa Sarah Bonvicini for having the charge of me during the process and helping me in any bureaucratic issue.

Second, I would like to thank Professor Valerio Cozzani for giving me the possibility of developing this thesis and to contribute with his knowledge to improve it. Moreover, I would like to thank Researcher Alessandro Tugnoli for helping me to structure the experiments and for his advice.

Third, I would like to thank Mercedes Gomez for both her time and help during the whole stage. I also thank Marco Muccini for his work with the tubular reactor, which made the thesis more accurate. In addition, I would like to thank all my mates from the DICMA department for their help and their support.

Thanks also to the *Universitat Politècnica de Catalunya* and the *Università di Bologna* for make this stage possible.

Finally, I would like to thank my family, my parents, my friends and Frederic Porta Serramià for encouraging me to embark in an international exchange.

INDEX

| | |
|--|----|
| 1. INTRODUCTION | 5 |
| 1.1. Passive Fire Protection | 5 |
| 1.2. Categories of fireproofing materials | 6 |
| 1.3. Typical Characteristics of fireproofing materials..... | 10 |
| 1.4. Objectives | 10 |
| 2. EXPERIMENTAL SECTION..... | 11 |
| 2.1. Instrumentation and techniques..... | 11 |
| 2.1.1. Thermogravimetric analyzer | 11 |
| 2.1.2. Fixed Bed Tubular Reactor..... | 12 |
| 2.1.3. Oven..... | 15 |
| 2.1.4. Scanning Electron Microscope..... | 16 |
| 2.2. Experimental Procedures | 17 |
| 2.2.1. Thermogravimetric analyzer..... | 17 |
| 2.2.2. Fixed Bed Tubular Reactor tests | 19 |
| 2.2.3. Sample conditioning | 22 |
| 2.3. Materials description..... | 23 |
| 2.3.1. Epoxy-based intumescent coating: Chartek7 TM | 23 |
| 2.3.2. Vermiculite-cement coating: Fendolite TM | 25 |
| 2.4. Materials characterisation..... | 26 |
| 2.4.1. Epoxy-based intumescent coating: Chartek7 TM | 26 |
| Characterization of high temperature exposure behaviour in TGA tests..... | 26 |
| Characterization of high temperature exposure behaviour in Fixed Bed Tubular Reactor tests | 27 |
| Characterization of high temperature exposure behaviour from morphological analysis..... | 34 |
| 2.4.2. Vermiculite-cement coating: Fendolite TM | 39 |
| Characterization of high temperature exposure behaviour in TGA tests..... | 39 |
| Characterization of high temperature exposure behaviour in Fixed Bed Tubular Reactor tests | 45 |
| Characterization of high temperature exposure behaviour from morphological analysis..... | 49 |
| 2.5. Degradation kinetic modelling for Fendolite TM | 52 |
| 2.5.1. TG tests used for the kinetic modelling | 52 |
| 2.5.2. Development of an apparent kinetic model..... | 57 |
| 3. CONCLUSIONS | 67 |
| 4. BIBLIOGRAPHY..... | 69 |
| APPENDIX A..... | 72 |
| APPENDIX B..... | 74 |

1. INTRODUCTION

1.1. *Passive Fire Protection*

Nowadays, there is an increasing concern about fires and mostly in process industries which use inflammable substances and could represent a high danger to workers and inhabitants from the surroundings as well as an economic damage by asset and material destruction.

Several studies have shown that, after contention losses, one of the most common accidents are fires (Casal et al., 1999). The next table shows the distribution of the number of industrial accidents. Fires are the second type of accidents which occur more frequently, just below by contention losses (Muñoz, 2005).

| Accident type | Occurrence percent (%) |
|-----------------|------------------------|
| Contention loss | 53.8 |
| Fire | 33.0 |
| Explosion | 26.4 |
| Non specified | 9.7 |
| Gas cloud | 7.7 |

Table 1 Occurrence of accidents in process industry

These accidental fires could result into more severe secondary events, causing a domino effect. This phenomenon consist of a propagation of accidental scenarios to equipment not directly involved in the primary accident and contemporary increasing the severity of the event (Cozzani et al., 2005)

Passive Fire Protector Materials (from now onwards PFP materials), or Passive Fireproofing Materials, are insulating systems used to protect industrial equipment against accidental fires, avoiding a rapid increase of temperature and a decrease of mechanical properties of the structural materials. If properly applied, this may prevent failures, losses of containment and accident escalation phenomena. Fireproofing is considered a passive protection barrier since it does not require manual, mechanical or other means of initiation, replenishment or sustenance. In this way, the adoption of fireproofing represents an important safety prevention measure against serious danger to human health and/or the environment as required by the Seveso Directives for major hazard installations.

Steel is a material commonly used in the process industry. It is a non-combustible material which exhibits a good ductility but it begins to lose its structural properties between 470 and 500°C. Due to this low failure temperature, the protection of materials against fire has become an important issue in

the industry. Indeed, prevention of the structural collapse of equipments, which can occur if load bearing steel elements reaches a temperature above 550°C, is necessary to ensure the safe evacuation of people from the surrounding areas. Similarly, steel vessel may lose their structural properties, leading to loss of the contained materials. If these are dangerous materials, domino escalation may occur. Actually a twofold phenomenon generally leads to failure of vessels exposed to fire: by one side the loss of structural properties of the heated steel weakens the structure, on the other the increase in internal pressure due to external heating rises the loads on the structure.

PFP materials create a low thermal conductivity layer, that protects the structure underneath from high flame temperatures. Some PFP materials may experience significant degradation during fire exposure, accompanied by devolatilization and variation of their physical properties. Moreover, they can hide the corrosion of the protected equipment and can be affected by the water supplied with high pressure on an emergency situation. Thus, the insulation should not be corrosive and should avoid the water to enter, if not, some protective layers can be used (primers and topcoat sealers). For that reason, sometimes a galvanized steel sheet cladding is used for covering the coatings. In addition, it should not be affected by the expansion/contraction of the protected material.

In order to model the performance of these materials, an investigation of their degradation behaviour is compulsory.

1.2. Categories of fireproofing materials

Several means exist for the protection of steel. These can be panels or blankets, but usually are mineral-based or organic resin-based coatings, such as intumescent ones. Intumescence is the swelling of certain substances when they are heated. Intumescent coatings form on heating an expanded multicellular layer, which acts as a thermal barrier that effectively protects the substrate against rapid increase of temperature, thereby maintaining the structural integrity of the building. (Jimenez et al., 2006).

The use of fire retardant coatings is one of the easiest, oldest and most efficient ways to protect a substrate against fire. In fact, it presents several advantages: it does not modify the intrinsic properties of the material, it is easily processed and may also be used onto several materials including metallic materials, polymers, textiles and wood.

When selecting a fireproofing material, the weight that the structure at high temperatures can support must be considered as well as the material adhesion strength, durability and the fire resistance rating required by the structure. The atmosphere where the coating will be located and the long-term performance/weathering, etc. should be also taken into account. Resistance to mechanical impact, abrasion and vibrations is also necessary. Some endothermic wrap systems and flexible epoxy

intumescent coatings can be useful in the accomplishment of this. The operating temperature limitation of the fireproofing materials shall be also considered.

There are several ways to classify the fireproofing materials. In the following the classifications proposed by a few authoritative sources are listed:

1. API14G-2007

The most used fireproofing materials are insulants. They can be classified in two groups: active and inactive insulants.

- *Active insulants* or intumescent materials undergo a physical and/or chemical change when exposed to heat, increasing their thickness thus providing enhanced insulation (i.e. ceramic fiber, epoxy-based matrix, etc.).
- *Inactive insulants* can be classified in two groups: cementitious materials (generally spray-applied) and man-made fibers (ceramic fiber, mineral wool).

2. UNI

- *Passive system for fire resistance* (Sistema Passivo per la Resistenza al Fuoco): materials or material combinations which do not change their physical characteristics when exposed to fire. Materials which release water can be included in this group.
- *Reactive system for fire resistance* (Sistema Reattivo per la Resistenza al Fuoco): materials or material combinations which change their physical characteristics due to a chemical reaction when exposed to fire. Example: intumescent materials.

3. Lees

- *Concrete* : lightweight aggregate concrete, or vermiculite cement
- *Magnesium oxychloride cement*: contains water of crystallization
- *Mastics*: a pasty material used as a protective coating or cement (asphaltic or vinyl acrylic, generally used as conventional insulators). In this category are included the intumescent materials.

There are also reactive fire resistant coatings:

- *Magnesium oxychloride coatings* lose their water when exposed to fire. They form a porous matrix which is resistant to impact, abrasion, weather and fire. They require metal lath reinforcement, are slightly corrosive and tend to lack of adhesion. They are not recommended to use directly on stainless steel and aluminium structures because they can cause corrosion. If used, a protective layer shall be put first.

- *Intumescent coatings* release cooling gases and form a thick foam when exposed to fire. A ¼ in layer can provide 1 h of protection. Some of them are flexible and designed for elasticity and vibration tolerance.
- *Subliming coatings* protect the substrate while they remain on it, maintaining the coated structure under the sublimation temperature. Examples: ThermoLag 330 (used in aerospace work, ThermoLag 440).

4. API 2218

Concretes

There are dense and lightweight concretes. Concretes can support fire impingement , thermal shock and direct hose streams, but allow corrosion, making necessary the use of primer and top coatings. They can be precast or formed in place.

- *Dense Concretes* absorb heat through an endothermic heat of reaction when chemically bound water is released. They need steel reinforcement.
- *Lightweight Concretes* have better fire protection properties than dense concrete, but are susceptible to mechanical stress.

Spray-Applied Fire-Resistive Materials (SFRM)

- *Subliming, Intumescent, and Ablative Mastics*

Mastics provide heat barriers through subliming, intumescent and/or ablative mechanisms (ablative mastics absorb heat as they lose mass through oxidative erosion). Some of them require primer (for bonding) and top coatings (for avoiding water penetrations). They are lightweight but can be affected by direct hose streams. Some of them tend to shrink when drying and require maintenance. The intumescent properties can cause that some parts of the substrate remain unprotected after the expansion (for example in the corners).

- *Intumescent Epoxy Coatings*

They can be described as a mix of thermally reactive chemicals in a specific epoxy matrix formulated for fireproofing applications. Under fire conditions they react to emit gases (which can be toxic), which cool the surface while a low density carbonaceous char is formed. This char then serves as a thermal barrier". They are lightweight and have good bonding, but can be affected by the hose streams. Some of them can support jet fire impingement. They do not cause corrosion. The application should be carried out by an expert.

– *Lightweight Cementitious Fireproofing*

It is mixture of Portland cement and a lightweight aggregate (vermiculite, perlite, etc.). It has relatively lightweight. It's good for exterior applications and supports cracks and impacts. It may not need a top-sealing coat.

Preformed inorganic units or masonry

– *Preformed Inorganic Panels*

They can be formed by cement and a lightweight aggregate or by compressed inorganic insulating material (i.e. calcium silicate) and are generally attached by fasteners. External weatherproofing may be required. They have low conductivity but can be affected by impacts.

– *Masonry Blocks and Bricks*

Masonry blocks: generally of lightweight blast-furnace slag joint by fireproofing mortar. Bricks are no longer used because their installation cost is high and they admit moisture, causing corrosion.

Endothermic Wrap Fireproofing

They absorb heat chemically (releasing water) and physically (the released water absorbs heat). It is a flexible sheet formed by an endothermic inorganic filler and an organic bonder. It can require substrate preparation for the application and a waterproof final layer. They can be applied over other fireproofing materials and are easily repaired.

In general dense concretes do not need their application by an expert, while the other materials should be applied by specialized team.

In this study, two reactive systems for fire resistance products will be tested: an epoxy-based matrix active insulant and a lightweight cementitious inactive insulant.

1.3. Typical Characteristics of fireproofing materials

In Table 2, there are the values of apparent density, thermal conductivity and the temperature where it was measured, of several insulating materials and compounds used in industry.

| | Apparent density at room temperature (kg/m ³) | T, °C | k (W/m k) |
|---|---|-------|-----------|
| Brick | 1842 | 800 | 1.0732 |
| Mineral wool | 150 | 30 | 0.0389 |
| Solid mica | 2800 | 50 | 0.4328 |
| Portland cement | 3000 | 90 | 0.2943 |
| Limestone (15,3 vol.% H ₂ O) | 1650 | 24 | 0.9347 |
| Asbestos-cement board | 1920 | 20 | 0.7443 |

Table 2 Apparent density, temperature and thermal conductivity for several insulating materials

Source: Perry's Chemical Engineer's Handbook, 8th edition

This values can be compared to those from air and water:

| | Apparent density at room temperature (kg/m ³) | T, °C | k (W/m k) |
|-------|---|-------|-----------|
| Water | 999.8 | 0 | 0.01574 |
| Air | 0.1745 | 1727 | 0.11675 |

Table 3 Air and water properties

Source: Perry's Chemical Engineer's Handbook, 8th edition

The best values are those which are lower, such mineral wool conductivity.

1.4. Objectives

In the current work, the degradation behaviour of commercial PFP materials exposed to high temperatures will be analyzed. Laboratory-scale experiments (Thermogravimetric (TG) techniques, fixed bed reactors, etc.) will be used at the scope. More concretely, the two commercial materials are investigated: an epoxy intumescent coating, Chartek7™, and a vermiculite based cementitious material, Fendolite™. The first one shows an intumescent behaviour while the second one does not.

First, the behaviour of the materials exposed to high temperatures will be analyzed. Then, the significant decomposition steps will be identified. In particular for the cementitious material, an apparent kinetic models will be developed for the description of the material degradation as a function of the temperature profile.

2. EXPERIMENTAL SECTION

2.1. Instrumentation and techniques

2.1.1. Thermogravimetric analyzer

The Thermogravimetric Analyzer (TGA) is a thermal weight-change analysis instrument which used in conjunction with a thermal analysis controller and associated software constitutes a thermal analysis system. The model used in current study is a TGA Q500 from the TA Instruments Company.



Figure 1 TGA Q500 with Autosampler

Source: TGA Manual Data Sheet

The Thermogravimetric Analyzer measures the amount and rate of weight change in a sample, either as a function of increasing temperature, or isothermally as a function of time, in a controlled atmosphere. It can be used to characterize any material that exhibits a weight change and to detect phase changes due to decomposition, oxidation, or dehydration. This information is useful to identify the percent weight change and correlate chemical structure, processing, and end-use performance.

The TGA components are:

- The balance, which provides precise measurement of sample weight. The balance is the key to the TGA system.
- The sample platform, which loads and unloads the sample to and from the balance.
- The furnace, which controls the sample atmosphere and temperature.
- The cabinet, where the system electronics and mechanics are housed.
- The heat exchanger, which dissipates heat from the furnace.
- The two mass flow controllers, which control the purge gas to the balance and furnace.

| | |
|-----------------------------------|---|
| Dimensions | Depth 55.9 cm Width 47 cm Height 52.1 cm |
| Weight | 30.9 kg |
| Weight of transformer | 8.18 kg |
| Power | 120 Vac, 50/60 Hz, standard 230 Vac, 50/60 Hz, if configured with a step-down transformer |
| Energy consumption | 1.5 kVA |
| Insulation Rating | All electrical insulation between hazardous components have been designed to meet the requirements of reinforced insulation. Low voltage circuits are grounded. |
| Room Operating Temperature | 15°C to 35°C (non-condensing) |
| Temperature control range | Ambient +5°C to 1000°C |
| Thermocouple | Platinel II |
| Heating rate | 0.1 to 50°C/min |

Table 4 Characteristics

Source: TGA Manual Data Sheet

2.1.2. Fixed Bed Tubular Reactor

The apparatus is an assembly of several components, as illustrated in Figure 2.

The heating system is a 1200°C tube furnace from the Carbolite Company with the characteristics reported in table 5. The model is HST 12/300 and the controller is W301. The furnace uses a voltage of 220V 1-phase. The whole system is formed by the furnace itself and a controller.



Figure 2 Tubular furnace

Source: Muccini 2011.

| MODEL | Max. Temp. (°C) | Max. Power (kW) | Work Tube Bore (mm) | Work Tube Length (mm) | Heated Length (mm) | Net Weight (kg) |
|------------|-----------------|-----------------|---------------------|-----------------------|--------------------|-----------------|
| HST 12/300 | 1200°C | 1.5 | 25-100 | 450 | 400 | 29 |

Table 5 Characteristics of the furnace in the fixed bed reactor assembly

Source: Tubular furnace Manual Data Sheet

The Fixed Bed Tubular Reactor equipment can be schemed as follows.

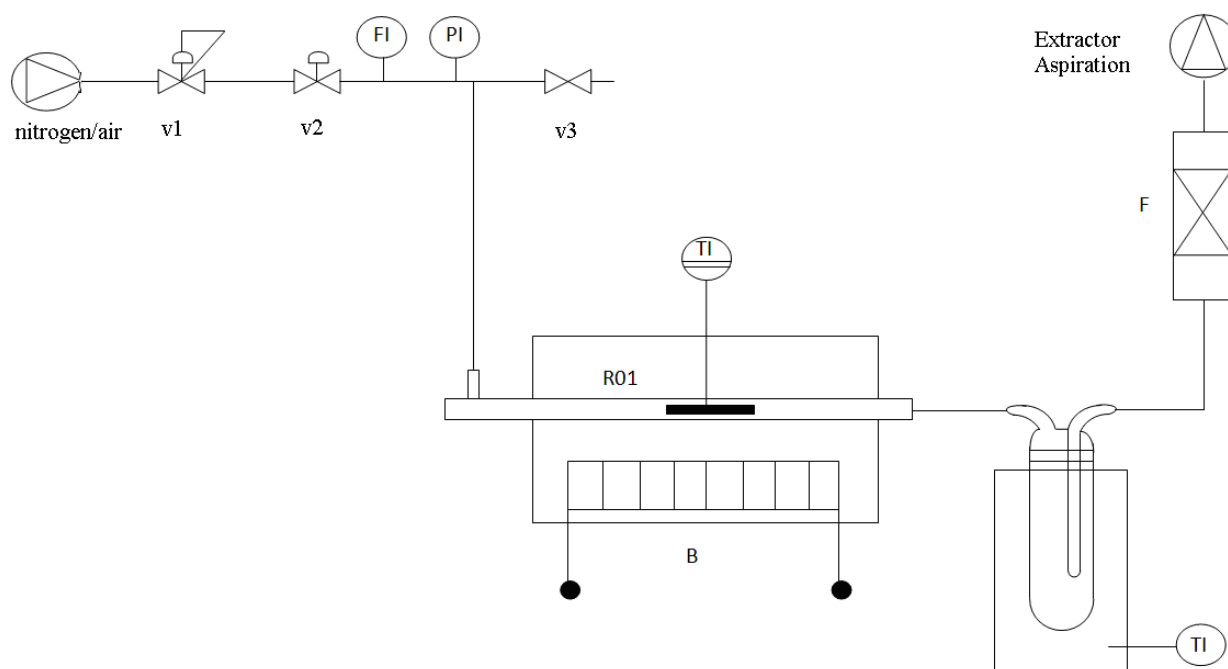


Figure 3 Installation scheme (Muccini, 2011)

The gas entrance is placed on the left side of the scheme. In order to control the pressure there is an auto-regulated valve, keeping constant downstream pressure.

The valve V1 is used to shift the gas flow, measured by means of a flowmeter with a floating ball (standard flow value: 1,4 NI/h). The pressure indicator PI allows to detect an eventual obstruction all along the gas circuit. In case of a pressure rise, the nearby discharge (V3) valve must be opened. It could be also necessary to switch off the installation in order to remove the internal obstruction.

The next section shows the reactor (R01) and the heating furnace (B). The reactor is constituted by a metallic tube 638mm long where is inserted, by means of a metallic pole, a sample-containing basket 125mm long. In this cavity are placed the thermocouples which are in contact with the sample in the spoon. At the beginning and at the end of the pole there are two heads which allow the reaction gas go

across. Moreover, at the end of the reactor a tube restriction 138mm long is placed in order to diminish the volume and pass-section of outgoing gas, thus reducing the temperature in the final reactor section. In this way it is possible to minimize secondary degradation reactions of gaseous compounds.

After the reactor, a sequence of cold traps is present (E) and an active carbon filter (F). The traps are used to condensate a fraction of the gaseous products. In fact, they are cooled by mixing ice with common salt (NaCl), obtaining a mixture which melting temperature is between -13 and -20°C. Then, it is possible to collect high condensable products and also avoid a condensation in a successive section of the circuit as well as the possibility of a later re-evaporation and return of the same compounds. The active carbon filter is used to guarantee a safety of the output gases.

After the traps and the filter, the process finishes with an extractor (Muccini, 2011).

The Eurotherm 301™ oven controller uses PID (Proportional Integral Derivative) temperature control, which uses a complex mathematical control system to adjust the power being sent to the heating elements and hold the furnace or oven at the desired temperature.





| | | |
|---------------------|---|---|
| Page Key |  | The <i>Page</i> key is used to scroll through the parameters and switch between menus. |
| Timer Key |  | The <i>Timer</i> key is used to start, view, pause and reset the timer. |
| Arrow Keys |  | The <i>Arrow</i> keys are used to adjust the value of the selected parameter and pause the output power. |
| Overtemperature Key |  | The <i>Overtemperature</i> key is used to access the Overtemperature menu. <i>Note: Overtemperature is an option</i> |

Figure 4 Temperature controller keys

Source: TGA Manual Data Sheet

2.1.3. Oven

This equipment is used for sample conditioning . It is constituted of a heating/drying oven with forced convection called APT.line™ FD from the Binder Company.

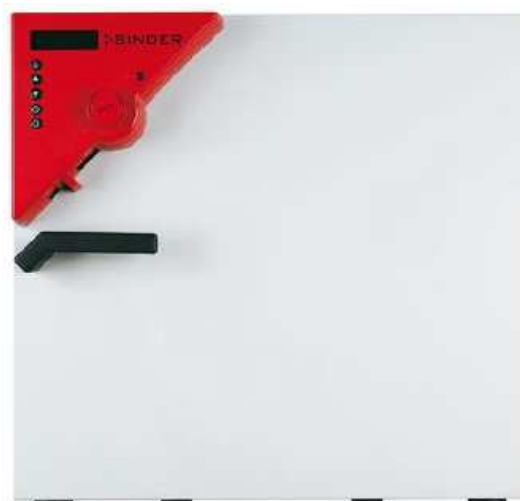


Figure 5 APT.line™ FD Oven

Source: Oven Manual Data Sheet

This oven is ventilated by fan-assisted, forced-air circulation. The temperature range is: 5°C above room temperature up to 300°C.

Temperature ramps can be programmed in order to extend heating up times. This may be necessary in some cases, in order to prevent temperature stresses in the material during the heating up phase.

| Exterior width (mm) | Exterior height (mm) | Depth (mm) | Interior width (mm) | Interior height (mm) | Depth (mm) | Interior volume (l) | Weight (empty) (kg) | Permitted total load (kg) |
|---------------------|----------------------|------------|---------------------|----------------------|------------|---------------------|---------------------|---------------------------|
| 634 | 617 | 575 | 400 | 400 | 330 | 53 | 44 | 40 |

Table 6 APT.line™ FD Oven - Dimension data

| Temp. range (°C) | Final temp. (°C) | Voltage (V) | Nominal power (kW) | Energy consumption (W) | | |
|-------------------------------|------------------|-------------|--------------------|------------------------|----------|----------|
| | | | | At 70°C | At 150°C | At 300°C |
| 5°C above ambient temperature | 300 | 230 | 1.2 | 172 | 429 | 951 |

Table 7 APT.line™ FD Oven - Temperature and electrical data

Source: Oven Manual Data Sheet

2.1.4. Scanning Electron Microscope

A Scanning Electron Microscope (SEM) was used in order to carry out a morphological analysis of Chartek7™ and Fendolite™.

The SEM is a type of electron microscope that images a sample by scanning it with a high-energy beam of electrons in a raster scan pattern. The electrons interact with the atoms that make up the sample producing signals that contain information about the sample's surface topography, composition, and other properties such as electrical conductivity.

In a typical SEM, an electron beam is emitted from an electron gun fitted with a tungsten filament cathode. Tungsten is normally used in thermionic electron guns because it has the highest melting point and lowest vapour pressure of all metals, thereby allowing it to be heated for electron emission, and because of its low cost.

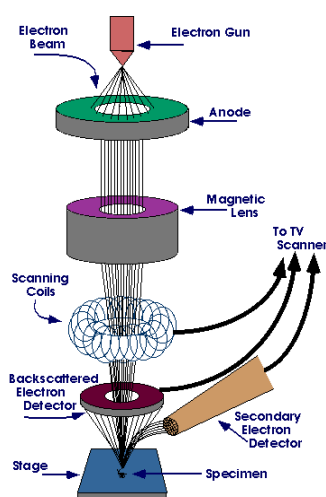


Figure 6 Diagram of SEM

Source: MicroTech Sciences Limited, 2007

The equipment used for the tests was the JEOL JSM 5600 LV. It is a high-performance scanning electron microscope with a high resolution of 3.0 nm. The PC Interface allows the instrument to be operated with a mouse only. The Low Vacuum mode, allows for observation of specimens which cannot be viewed at high vacuum due to excessive water content or due to a non-conductive surface. Its specimen chamber can accommodate a specimen of up to 6-inches in diameter and its standard automated features include Auto Focus/Auto Stigmator, Auto Gun (saturation and alignment), and Automatic Contrast and Brightness. Specifications: Resolution: High Vacuum mode: 3.0 NM (30kV, WD8mm, SEI), Low Vacuum mode: 4.5NM (30kV, WD5mm, BEI). Accelerating voltage: 0.5 to 30 kV (53 steps). Magnification: x 18 to 300,000 (136 steps). Objective lens: Conical lens. Objective lens apertures: Click-stop type (3-step variable). Fine position. controllable in X/Y directions. Maximum specimen size: 6-inch (150.0mm) dia (Università di Pisa).

2.2. Experimental Procedures

2.2.1. Thermogravimetric analyzer

2.2.1.1. TGA Calibration

The instrument should be calibrated in order to obtain accurate experimental results. It is recommended to recalibrate it periodically.

Two types of calibration are needed for the TGA: temperature and weight calibration.

Temperature calibration is useful for TGA experiments in which precise transition temperatures are essential.

Weight calibration should be performed on the TGA at least once a month. The weight calibration procedure calibrates both the 200 mg and 1g weight ranges. The calibration parameters are stored internally in the instrument. The calibration uses two reference calibration weights to tune the weight sensor. The exact weight of the calibration weights must be determined before they are used to calibrate the instrument.

Temperature calibration tunes the temperature sensor in the furnace in a way that it can be good representation of the sample temperature. Calibration is based on the Curie temperature of reference samples. Curie temperature is measured detecting apparent weight change of a sample in a magnetic field. In order to carry out the TGA temperature calibration it is needed to analyze a high-purity magnetic standard considering its Curie temperature, and then enter the observed and real values in the temperature calibration table. The observed and real temperatures correspond to the experimental and theoretical transition temperatures. From one to five temperature calibration points (pairs of observed and actual temperature points) can be entered in the calibration table. A multiple-point calibration is more accurate than a one-point calibration.

During this work, temperature calibrations tables were defined for the following set of constant heating rates:

- 5°C/min,
- 10°C/min,
- 25°C/min and
- 45°C/min,.

2.2.1.2. TGA Experimental procedure

Several TGA runs were carried out during the experimental activities. All of the TGA experiments have the following general procedure:

- Opening the gas valves (nitrogen and pure air).
- Setting name and file.
- Tare of the empty sample pan.
- Loading the sample into the pan.
- Defining experimental program of the test.
- Running the experiment.
- Cooling and discharging of the sample.
- Cleaning the pan.

The tare operations guarantees that the measured weight is the one of the sample only. The sample load must be done ensuring that the thermocouple does not touch the sample. During the whole process, brass tweezers must be used to handle the sample pans.

Several programs were followed during the tests. Two main families can be identified. First, those were a heating ramp of 5, 10, 25 and 45°C/min was applied until 950°C. Second, the isothermal tests were set-point temperature is reached as quickly as possible and then maintained.

For example, in case of 10°C/min ramp, the experimental program was:

- Data storage on: begin data storage
- Equilibrate at 30°C: to remove initial moisture
- Ramp 10°C/min to 800°C: heating process
- Isothermal for 10min: to completely achieve the final temperature
- Select gas 2 (air): in order to burn the organic compounds (in case there is any)
- Isothermal for 10min: to complete the oxidation process
- Data storage off: finish data storage
- Equilibrate at 100°C: in order to begin a new test at lower temperature

All the experiments were listed in a notebook containing several data as date, name, sample weight, procedure, etc. (see appendixes A and B). In this way all the tests could be planned and correctly managed.

The calibration procedures were also written down as well as the calibration temperature tables.

2.2.2. Fixed Bed Tubular Reactor tests

The Fixed Bed Tubular Reactor tests used the assembly described in section 2.1.2.

Standard samples of Chartek7™ used in the test, had the following characteristics:

- Geometric shape: parallelepiped
- Length: 90÷120 mm
- Width: 17÷20 mm
- Weight: 15÷22 g

Dealing with Fendolite™, the same procedures were followed using standard samples:

- Geometric shape: parallelepiped
- Length: 90÷120 mm
- Width: 20÷22 mm
- Weight: 11÷24 g

Generally, and in particular for Fendolite™ samples, the test samples were conditioned (see 2.2.3) prior to Fixed Bed Tubular Reactor tests.

The aim of these tests is exposing the samples to a prefixed thermal program in controlled atmosphere. Both burned samples and the compounds collected in the traps can be regained. At the end, the samples can be quantified and analyzed.

The data obtained from the tests are registered in tabs. The key information is:

- Test identification: name, operator, date, time, code.
- Initial type of material, shape, weight and dimensions.
- Relative position of the furnace and the thermocouples respect to the reference system of the reactor.
- Thermocouples type and dimension.
- Traps ice-bath temperature.
- Flushing gas type, flow and temperature.
- Thermal program description
- Residue weight, shape and dimensions.
- Trapped liquid weight and volume (if present).

This way, it is possible to register a clear reference of all the tests. Moreover, an automatic file is created containing a continuous register of the thermocouples temperature. A data logger (Argilent) is set to perform four scans per second for each of the two thermocouples.

The experimental procedures consist of the next steps:

- Switch on the furnace.
- Assembly of the various parts of the spoon and the furnace, and thermocouples insertion.
- Weigh of the empty traps.
- Assembly of the out-put gas circuit (trap cooling mixture preparation, trap and cooling mixture collocation, circuit connexion).
- Weigh and measurement of the sample.
- Setting the sample into the spoon and introducing altogether inside the tubular reactor.
- Setting the thermal program.
- Start test

At the end of the test:

- Pull the sample out the furnace hot area.
- Trap isolation and weigh.
- Cool the sample by means of a gas flow till a temperature lower than 200°C.
- Regain of the solid sample: sample weigh and measurement, regain of the micro-samples (ca. 10 mg) in order to carry out a thermogravimetric analysis (TGA).
- Regain of the liquid samples collected in the traps and volume measurement.
- Disassembly and cleaning the equipment.

The furnace spoon has to be collocated in the reactor tube paying attention not to over-turn the sample. The sample must be touching the thermocouples inside the spoon. This one is located in a specific zone of the furnace where the temperature profile has been previously measured to be uniform.

The ice mixture used to cool the cold trap was crushed and mixed with salt to diminish the temperature. The glass trap, where the vapours will condensate, is inserted into a Dewar container filled with the ice mixture. The trap is connected to the reactor by silicon rubber tubes. The liquid condensed in the trap can be recovered for further analysis.

In current setup, the possible gas supply are dry air and nitrogen, both technical grade.

Thermal programs

Each test can follow two types of thermal program:

1. Thermal program 1: sample heating till a desired temperature following a 10°C/min ramp. When the thermocouple temperature is the same of the maximum chosen temperature, the sample is removed from the furnace hot area and cooled, always in an inert atmosphere, till 200°C.

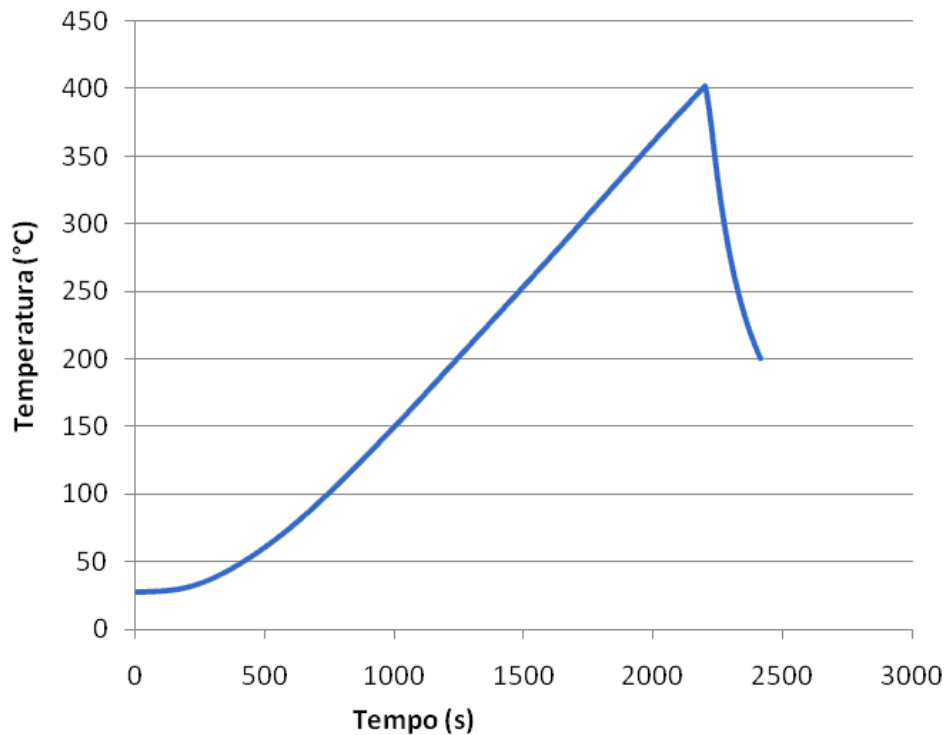


Figure 7 Thermal program 1. Heating till 400°C, sample removal from hot area and cooling till 200°C
Source: Muccini, 2011

2. Thermal program 2: sample heating till a maximum desired temperature following a 10°C/min ramp. When the controller achieves the chosen temperature (it would be different from this of the thermocouples), it sets an isotherm of a chosen length, at the end of whom the sample is removed from the hot area of the furnace.

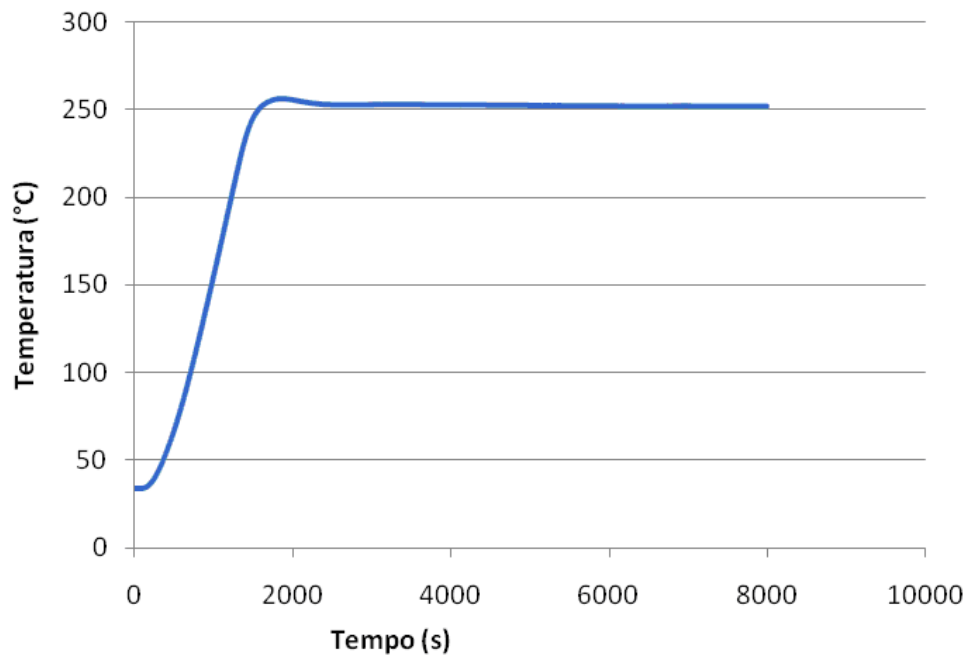


Figure 8 Thermal program 2. Heating till 250°C and 2-hour-isotherm at the same temperature. The final cooling till 200°C is not plotted but it is done.

Source: Muccini, 2011

2.2.3. Sample conditioning

Some samples, especially of Fendolite™, resulted sensitive to the amount of humidity present in ambient air. Thus a sample conditioning protocol was defined.

The protocol consist in maintaining the sample at a fixed temperature for at least 24h in the ventilated oven. For Fendolite™ optimal results were obtained at 110°C for 24h.

Conditioned samples are generally used as soon as withdrawn from the oven. For longer waiting timed a exsiccator with silica gel was used.

2.3. Materials description

2.3.1. Epoxy-based intumescent coating: Chartek7™

The material is a high performance epoxy intumescent fire protection coating system. It is suitable for the protection of steel, aluminium and other substrates from the effects of hydrocarbon pool and jet fires. The material is applied with spray methods.

The material is a mixture of several components. Notably, it contains flame retardants: a mineral acid (boric acid, H_3BO_3) and ammonium polyphosphate ($(NH_4)_{n+2}P_nO_{3n+1}$, APP) derivative (Jimenez et al., 2008).

Some physical and chemical properties are (Reynolds et al., 1992; Chartek7 data sheet):

- Tested apparent density: 1165.4 kg/m^3
- Solubility in water: immiscible
- Thermal conductivity (k): 0.24234 W/m K
- Specific heat capacity (Cp): 1967.8 J/kg K

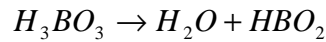
When the temperature of the coating reaches a critical temperature when exposed to the heat of the flame, the material is converted into highly viscous liquid. Simultaneously, reactions are initiated resulting in the release of gases. These gases are trapped inside the viscous fluid (formation of bubbles). The result is the expansion or foaming of the coating, sometimes up to several times its original thickness, to form a protective carbonaceous char that acts as an insulative barrier between the fire and the substrate.

Generally, three intumescent ingredients can be identified: an acid source, a carbon source and a blowing agent. The mechanism of intumescence is usually described as follows: first, the acid source breaks down to yield a mineral acid, then it takes part in the dehydration of the carbonization agent to yield the carbon char, and finally the blowing agent decomposes to yield gaseous products. The latter causes the char to swell and hence provides an insulating multi-cellular protective layer. This shield limits at the same time the heat transfer from the heat source to the substrate and the mass transfer from the substrate to the heat source resulting in a conservation of the underlying material. (Jimenez et al., July 2006).

Two different phases were described for swelling of intumescent materials (Jimenez et al., July 2006).

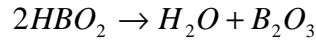
In the first phase, two main decompositions occur.

1. From 90°C to 140°C: Dehydration into metaboric acid:



Equation 1

2. From 140°C to 260°C: Dehydration of metaboric acid into boron oxide:



Equation 2

B_2O_3 is a very hard glass which crystals begin to break down at 300°C forming suboxides which melt at 700°C. As boric acid releases water and forms a hard glass, it can play the role of blowing agent which provides structural integrity to the char.

The second phase corresponds to the degradation of the epoxy resin and APP (Jimenez et al., 2008). Pure APP starts losing ammonia at temperatures higher than 200°C forming phosphoric acid. Boron oxide and APP may react yielding borophosphate.

The char of resin mixed with boric acid has an excellent mechanical resistance. Moreover, borates provide the good structural properties of the char, whereas the phosphorus ensures the adhesion of the char on the steel.

2.3.2. Vermiculite-cement coating: Fendolite™

The product is an Spray-Applied Fire Resistive Material (SFRM) based on vermiculite, a type of mica, and Portland cement, as well as ground limestone. It is specifically developed for spray application to structural columns and beams in exterior environments and interior situations where higher levels of abrasion resistance and hardness are necessary.

Although Fendolite™ is 1/3 the density of regular concrete, thus significantly reducing dead load, it is also highly durable and resistant to cracking under mechanical impact. Some physical and chemical properties are:

- Tested apparent density: 732 kg/m³.
- Thermal conductivity: 1.32 BTU in/hr ft² °F @ 75°F / (0.19 w/mK @ 24°C)
- Compressive Strength: 78,912 psf (3,778kPa)
- Cohesion/adhesion: 11,870 psf (568kPa)

It contains a great quantity of cement, i.e. maximum 60%, and the other compounds are often insulating materials as mica and aggregates as ground limestone which give insulation without adding significant weight to the structure.

Mica is added in order to increase insulating properties without increasing weight, since mica is a light mineral. The material shows the behaviour of a common cement and the presence of air-filled pores yields a heat insulating barrier.

Several reactions take place during the heating process: water release, deshydroxilation and decarbonation, thus CO₂ is released. All these changes were observed during the material characterisation (see 2.4.2).

When heated, there is not an intumescent behaviour, thus there is not an important volume variation.

As cement is a cheap product, the resultant material is a good alternative since gives an appropriate response to fire without increasing price.

2.4. Materials characterisation

2.4.1. Epoxy-based intumescent coating: Chartek7™

Characterization of high temperature exposure behaviour in TGA tests

As could be seen in section 2.3.1., several reactions occur when Chartek7™ is exposed to high temperatures.

Figure 9 shows two different regions where several reactions take place when a chunk sample is degraded in a nitrogen atmosphere in the TGA at different heating rates.

As mentioned in section 2.3.1., the first reaction considers the degradation of the boric acid. It takes place in two different steps:

1. Between 90 and 140°C: dehydration of the boric acid into metaboric acid.
2. Between 140 and 260°C: dehydration of metaboric acid into boron oxide.

The second region, from 260-500°C, includes the degradation of the APP and the epoxy resin, occurring the material expansion from 260 to 400°C.

The final residue is about 35 % of the initial sample weight.

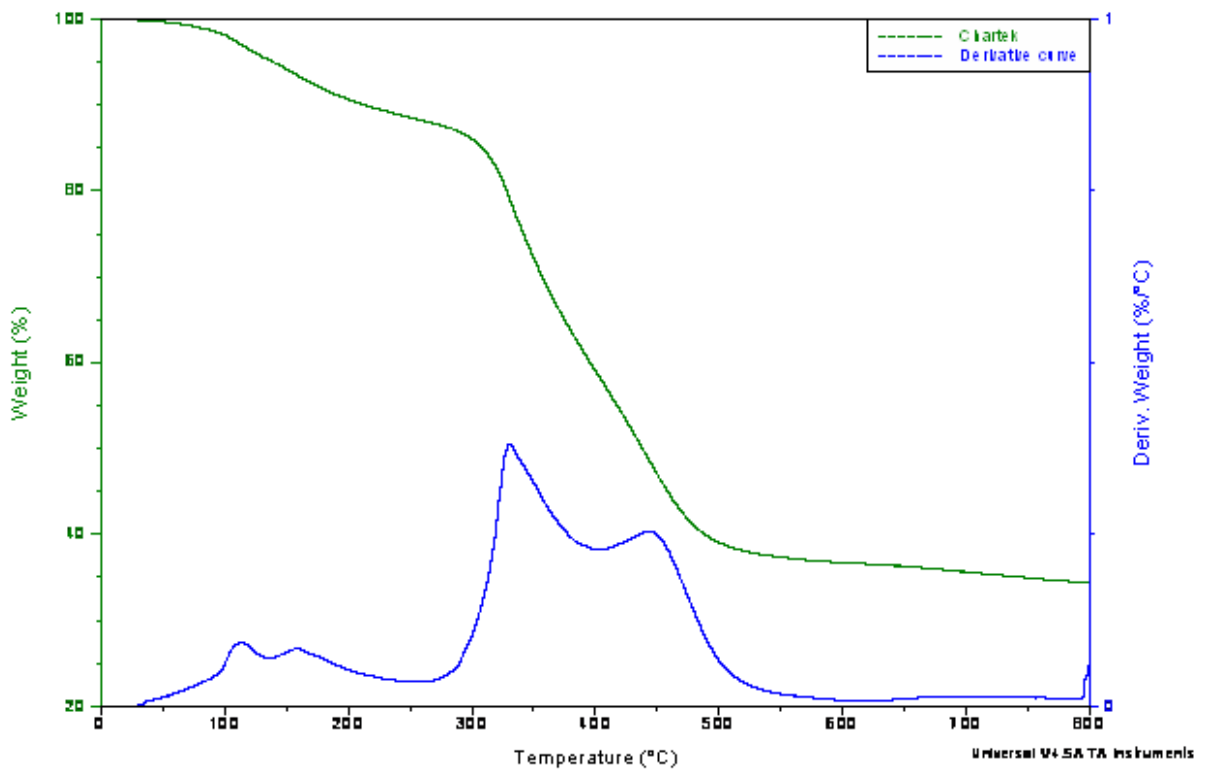


Figure 9 TGA of chunk Chartek7 samples with different weights using nitrogen

Source: Gomez-Mares

Characterization of high temperature exposure behaviour in Fixed Bed Tubular Reactor tests

Several Chartek7™ samples were exposed to different temperatures in a tubular reactor. Figure 10 shows different burning grades.



Figure 10 Degraded epoxidic resin at: a) 800°C, b) 600°C, c) 400°C, d) 350°C, e) 325°C, f) non-degraded

Three main aspects were taken into account: weight loss, comparison between tubular reactor and TG, and description of the substances collected in the traps.

– *Weight measurement before and after degrading:*

The sample always follows a type 1 thermal program (see section 2.2.2.). The different set point temperatures were chosen according to output results from the TGA. First, the sample was tested just above 200°C, then at 300, 400, 600 and, finally, at 800°C.

Figure 11 reports the weight loss as a function of the maximum temperature at which the sample has been exposed. The weight loss (WL) can be calculated as:

$$WL = 1 - \frac{w_f}{w_i}$$

Equation 3

Where w_f and w_o are the final and initial weight, respectively.

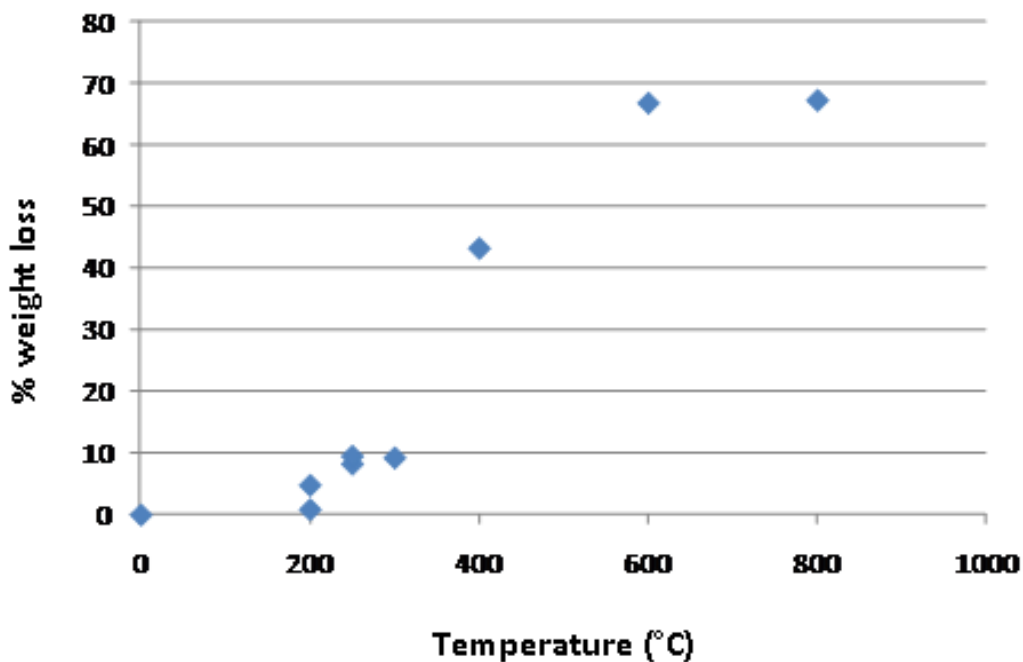


Figure 11 %Weight loss as a function of temperature

Source: Muccini, 2011

As can be seen in Figure 11, the sample suffers low weight loss till the 300°C. These results are in accordance with those from the TGA and can be interpreted as water release from boric acid decomposition. From this temperature onwards, the sample losses weight more substantially in the 300-400°C range. Here the weight percentage changes from 10% to 40%. According to the TGA results, at this range the main degradation of the Chartek7™ matrix takes place.

In the 400-600°C range the sample losses weight at a lower rate, reaching over a 67% of the sample which remains the same also when heating at 800°C.

As a conclusion, the maximum weight loss is about a 67% of the initial weight, agreeing with the TGA results, where the loss was the 65% of the original sample.

– Tubular reactor and TG comparison:

The aim is to confirm whether the two used test scales (TGA and tubular reactor) yield compatible results. A first step is comparing the weight loss for both tests. Figure 12 compares the residues from the TG and the tubular reactor.

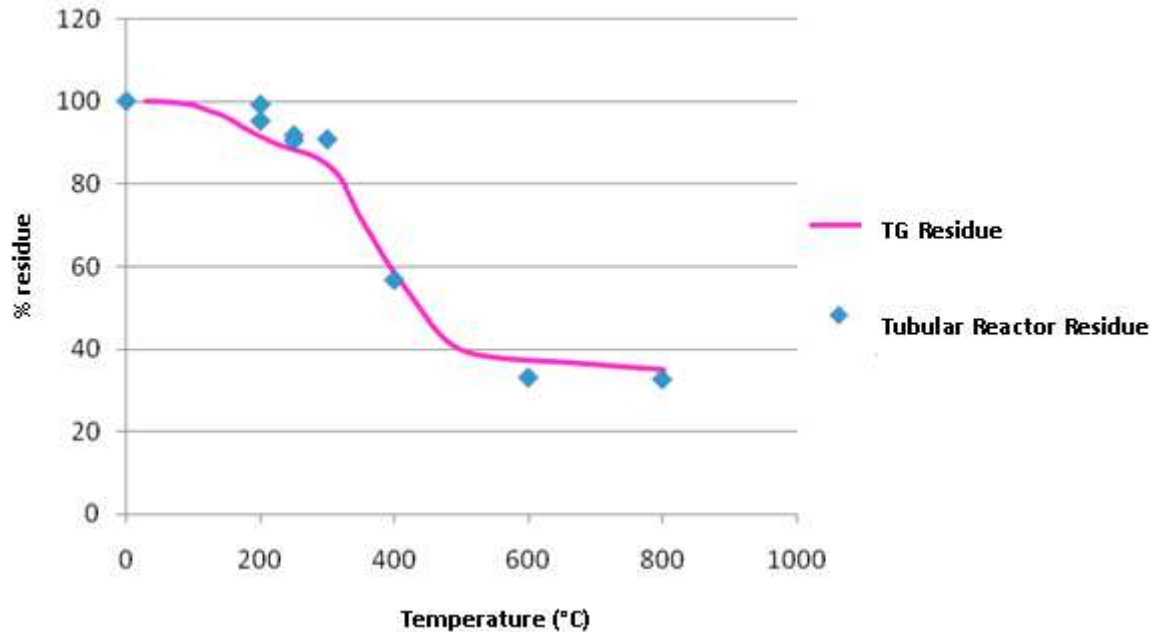


Figure 12 Residue comparison: TG and tubular reactor
Source: Muccini, 2011

Figure 12 shows that the results obtained from the tubular reactor are mainly the same than those from the TG curves. Thus, both tests can be correlated, at least when referring to weight loss.

A second step consist of extracting a sample from the solid residue obtained in the tubular reactor, and analyze it with the TG. This allows for verification of two facts:

1. Consistence of the weight loss for both tests.
2. Same degradation behaviour at higher temperatures than that reached.

Figure 13 shows several weight loss curves from the TG as a function of temperature, obtained by samples extracted from the tubular reactor at different final temperatures. In the same figure, the dots on the left axis report the final residue weight as measured from tubular reactor test.

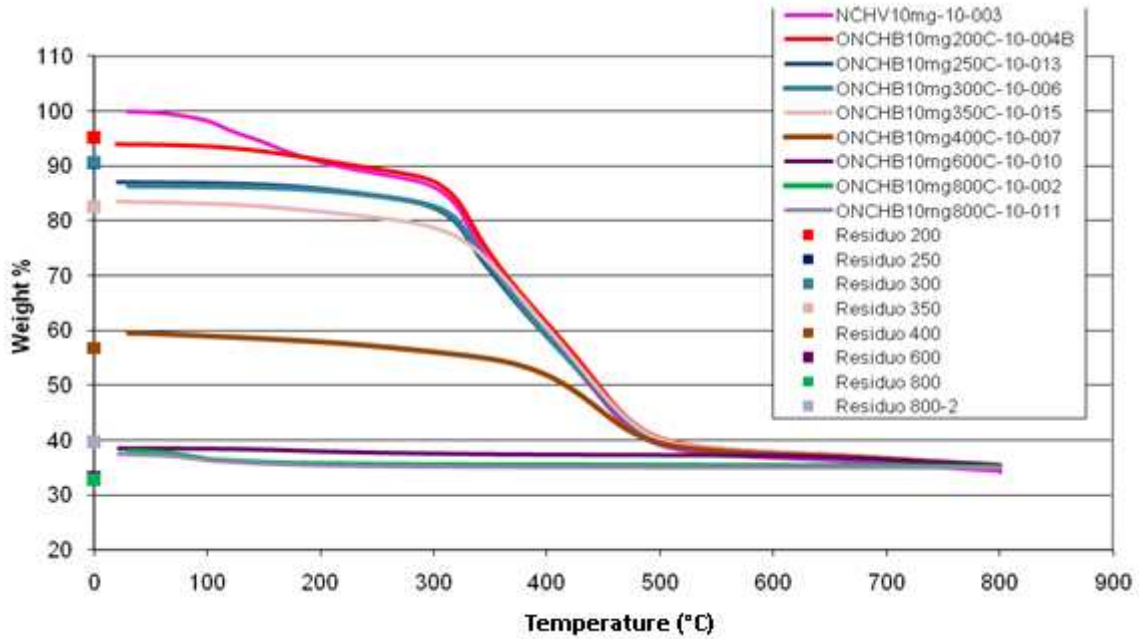


Figure 13 TG and tubular furnace tests

Source: Muccini, 2011

The thermal program followed in the TG used the same heating rate that in the furnace, i.e. 10°C/min, and it was of the type 2 (see section 2.2.2.). The output curves of the TG were rescaled in order to be represented in Figure 13. It was considered that all the TG tests had a residue of 35% at 800°C. All the values were thus recalculated as follows:

$$w_r = \frac{w_x \cdot 35}{w_f}$$

Equation 4

Where w_r , w_x and w_f are the sample weight rescaled, initial and final, respectively.

The points in the left represent the %weight loss measured in samples extracted from the furnace and are used to verify that during the time between the furnace extraction and the test in the TG, there were not remarkable weight variations. The similarity of the furnace points and the beginning of the rescaled TG curves confirms the weight loss consistence between both tests.

It can be seen as the curves behave in the same way at temperatures higher than the maximum test temperature. Moreover, all the curves are below the virgin sample tested, thus the results are correct.

As a conclusion, Chartek7™ test results obtained by TGA and tubular reactor are proved consistent and can be integrated in future degradation studies of the material.

- *Description and amount of condensable product collected in the traps:*

Table 8 shows several data from the collected liquids in the traps during tubular reactor tests on Chartek.

| Test identification | T (°C) | Initial weight (g) | Sample weight loss (%) | Condensable weight over initial sample weight (%) |
|------------------------|--------|--------------------|------------------------|---|
| NCHV22g10Cmin-800C-002 | 800 | 22.24 | 67.18 | 47.89 |
| NCHV16g10Cmin-600C-001 | 600 | 16.38 | 66.73 | 45.12 |
| NCHV18g10Cmin-400C-001 | 400 | 18.96 | 43.20 | 24.63 |
| NCHV16g10Cmin-300C-001 | 300 | 16.01 | 9.24 | 5.00 |
| NCHV18g10Cmin-250C-001 | 250 | 18.44 | 8.24 | 2.82 |

Table 8 Trap liquid information

Five tests at different temperatures were analyzed. In these tests, the formation of two different liquid phases was observed. The first one was transparent and was collected in all the tests above 250°C. The second phase was dark and viscous and it was observed only in the test where temperature was at least 400°C (Figure 14).

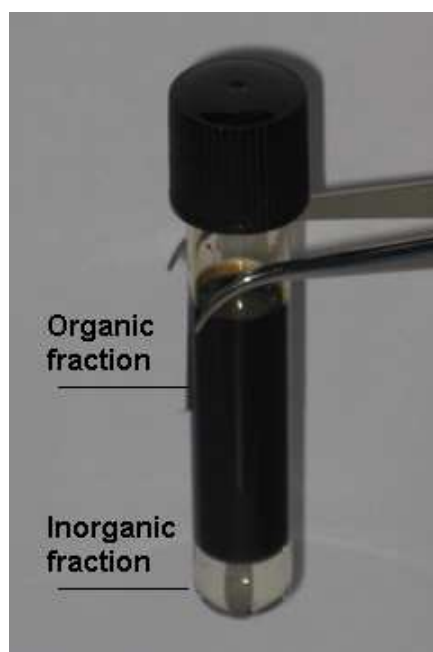


Figure 14 Liquid fractions collected in the traps

The transparent phase is very likely to be water, since the dehydration reaction of the boric acid finishes at about 260°C. The odour suggests traces of ammonia. The characteristics of the second phase lead to consider organic compounds.

The relation among the condensable and incondensable fractions is clearly dependent on the trap temperature. It is considered that the non-condensable fraction is constituted only of light gases, as CO₂ and NH₃. Table 9 shows the amounts of inorganic and organic liquid collected in traps.

| Test name | Inorganic phase volume (mm ³) | Organic phase volume (mm ³) |
|------------------------|---|---|
| NCHV22g10Cmin-800C-002 | 1700 | 7000 |
| NCHV16g10Cmin-600C-001 | 1000 | 5000 |
| NCHV18g10Cmin-400C-001 | 1400 | 2500 |
| NCHV16g10Cmin-300C-001 | 700 | 0 |
| NCHV18g10Cmin-250C-001 | 500 | 0 |

Table 9 Liquid volumes collected in the traps

As can be seen, tests carried out below 300°C do not yield organic product, since the main degradation reaction has not begun yet and the only produced substance is probably water from boric acid decomposition.

When rising the temperature, the amount of collected organic product does so. The quantity of collected liquid was lower than the total weight measured in the traps at the end of the tests, since there was a loss when emptying the traps and filling the graduated test tubes. The liquid phases mass fraction was estimated considering a reference density of 1000 kg/m³ for the inorganic phase (hypothetically water based) and of 850 kg/m³ for the organic phase.

Table 10 summarize the results obtained:

| Test name | M% tot. Inorganic | M% tot. Organic |
|------------------------|-------------------|-----------------|
| NCHV22g10Cmin-800C-002 | 11% | 37% |
| NCHV16g10Cmin-600C-001 | 9% | 37% |
| NCHV18g10Cmin-400C-001 | 10% | 15% |
| NCHV16g10Cmin-300C-001 | 5% | 0% |
| NCHV18g10Cmin-250C-001 | 3% | 0% |

Table 10 Percentage of liquid respect to the sample initial weight

As can be seen in Table 10, the amounts of collected water increase until their maximum at 400°C. This agrees with the predictions: above 300°C all the water has been released, this can be totally collected only at about 400°C. Moreover, above 600°C the organic fraction is almost constant, thus the degradation is finished over this temperature. The results confirm literature information regarding to the boric acid dehydration. At higher temperatures it is possible to recover the residues coming for the other degradations (APP and epoxy resin).

In

Figure 15, the distribution of the solid and liquid fraction are shown.

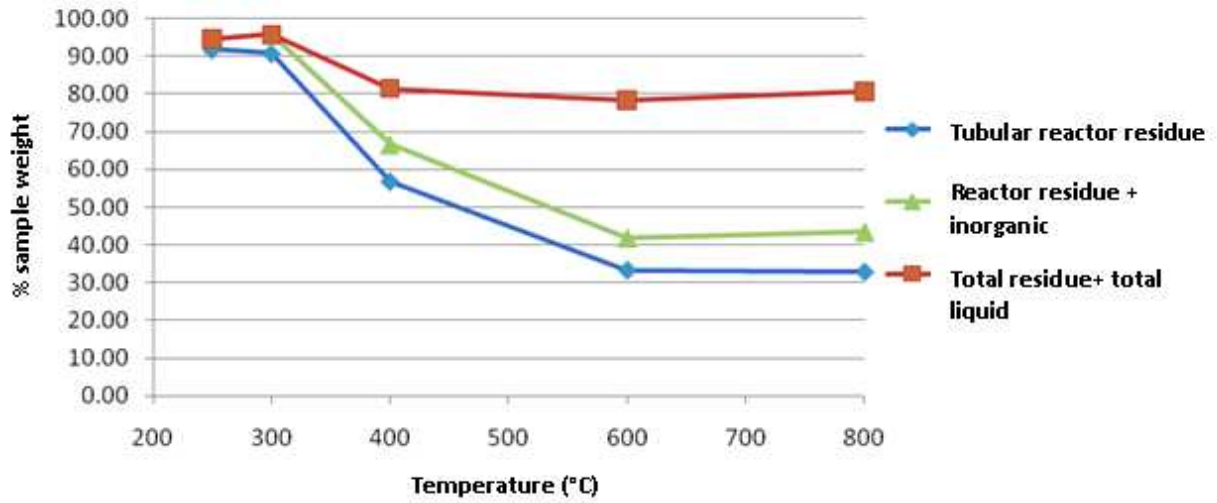


Figure 15 Solid and liquid distribution

Figure 15 provides at glance a visualization of the described phenomena. The blue curve represents the solid residue, the green one the solid plus the inorganic residues, while the red one represents the total liquid residue plus the solid one. Then, the area between the blue and green curves represents the amount of inorganic liquid, while the area located between the green and the red ones shows the amount of organic liquid. In addition, the section between the red curve and the 100% of the initial weight curve represents the amount of lost gas. Observing that the inorganic residue curve is parallel to the solid residue curve for temperatures higher than 300°C, it can be concluded that after that temperature, inorganic liquid is no longer formed. Similarly, organic liquid increases with final temperature only until reaching 600°C.

Characterization of high temperature exposure behaviour from morphological analysis

A Scanning Electron Microscope was used in order to carry out morphological analysis of samples from Fixed Bed Tubular Reactor tests. Both virgin and degraded material were studied.

– *Virgin material:*

Figure 16 shows the image of a virgin Chartek7™ sample obtained from SEM.

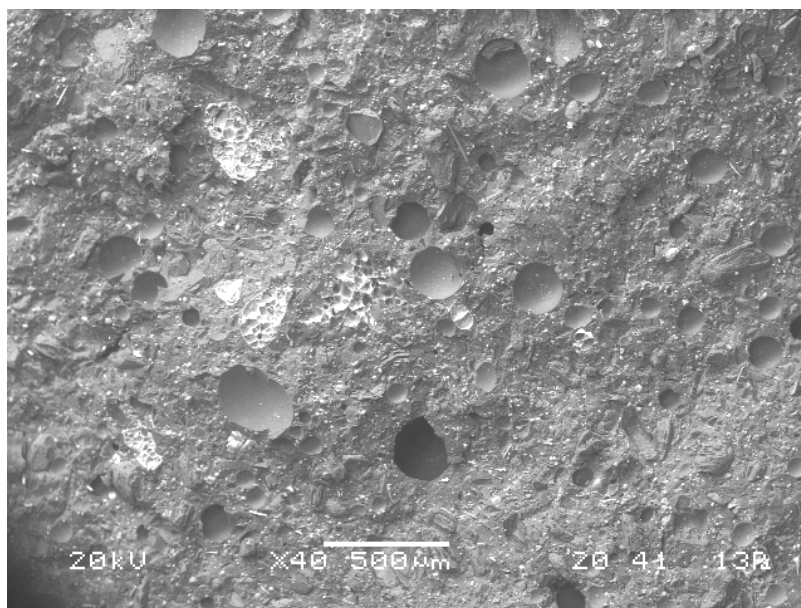


Figure 16 Virgin Chartek7 sample analyzed in SEM

There can be seen different heterogeneous phases in the material. Table 11 shows the average composition of the photographed area above.

| | %Weight | %Atomic |
|--------------|----------------|----------------|
| C | 35.89 | 44.98 |
| O | 52.96 | 49.82 |
| Al | 0.48 | 0.27 |
| Si | 3.18 | 1.70 |
| P | 4.20 | 2.04 |
| Ca | 2.46 | 0.92 |
| Ti | 0.84 | 0.26 |
| Total | 100.00 | |

Table 11 Composition of material from figure 12

First, oxygen and carbon referred to the epoxy organic matrix can be seen. Moreover, there are other elements as phosphor, aluminium, silicon and titanium. Phosphor derives from the ammonia polyphosphate (APP) which can be found in the material. The other elements can be attributed to the

inorganic filler. The instrument can not detect the presence of lighter elements, as hydrogen, boron, nitrogen, etc.

Figure 17 shows an higher magnification of the material, in order to better recognize the different phases.

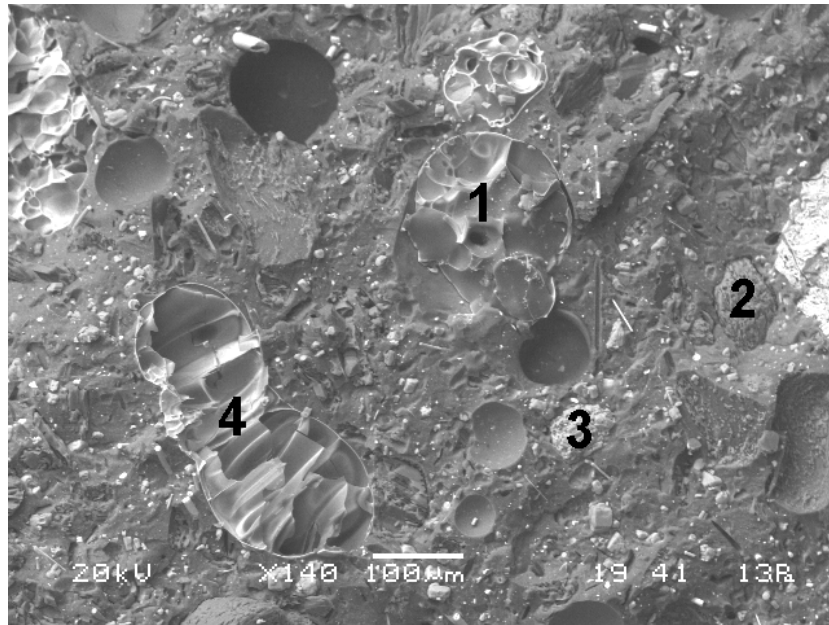


Figure 17 Chartek7™ magnified picture

The elementary composition analysis allows the knowledge of the material formulation. Table 12 shows the different values of %weight referred to the different areas indicated in Figure 17.:

| | 1 | 2 | 3 | 4 |
|--------------|-------|--------|--------|--------|
| C | 32.24 | 4.85 | 18.18 | 41.27 |
| O | 48.33 | 92.98 | 52.71 | 37.35 |
| Al | 1.30 | | | 2.32 |
| Si | 7.62 | 1.18 | | 14.86 |
| P | 3.95 | 0.62 | 29.11 | 1.53 |
| K | 1.26 | | | 2.18 |
| Ca | 3.30 | 0.38 | | |
| Ti | 2.00 | | | |
| Na | | | | 0.49 |
| Total | 100.0 | 100.00 | 100.00 | 100.00 |

Table 12 %Weight for the different areas

Point 1: the high amount of silicon suggests the presence of some kind of glass. The particles can be interpreted as sand used as a filler.

Point 2: the high oxygen concentration, the absence of other major elements and the impossibility of the instrument to detect hydrogen and boron leads to consider the particle as a boric acid crystallite, likely contained in the material according to literature.

Point 3: high phosphorus and oxygen concentrations indicate the presence of a phosphate, likely ammonia polyphosphate. Also this compound is contained in the Chartek7™ formula according to literature.

Point 4: high silicon and oxygen concentrations are detected, thus there is another glass agglomerate.

In some particles, as the none showed in Figure 18, there are high oxygen and calcium concentrations, which indicate the likely presence of calcium carbonate (CaCO_3), used as a filler. In the same figure, the glass fibers can be recognized, also used as a filler.

The high presence of all these inorganic phases used as a filler matches with the TGA tests, where the final residue appears as a significant fraction (35 %) and stable to oxidation above 800°C.

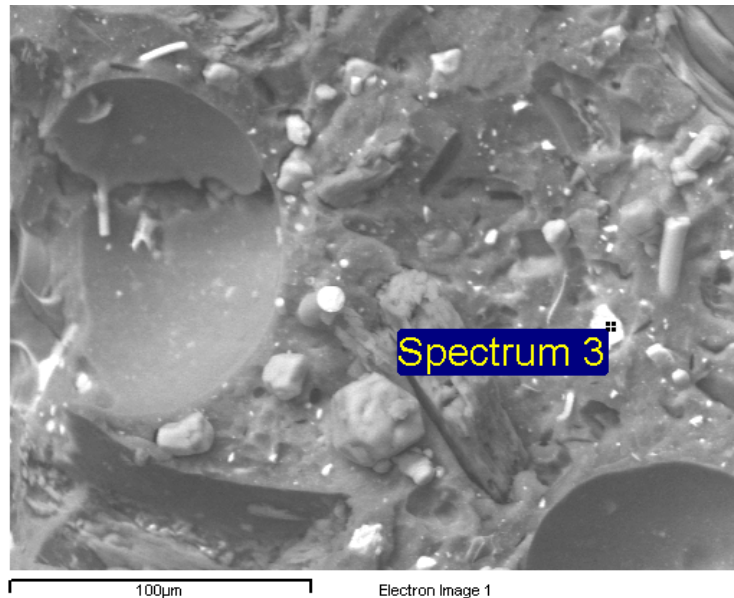


Figure 18 Particles of calcium carbonate

– *Degraded samples:*

Several 800°C-degraded samples were analyzed. Figure 19 reports a SEM image of a degraded sample whilst Figure 20 shows a particle magnification.

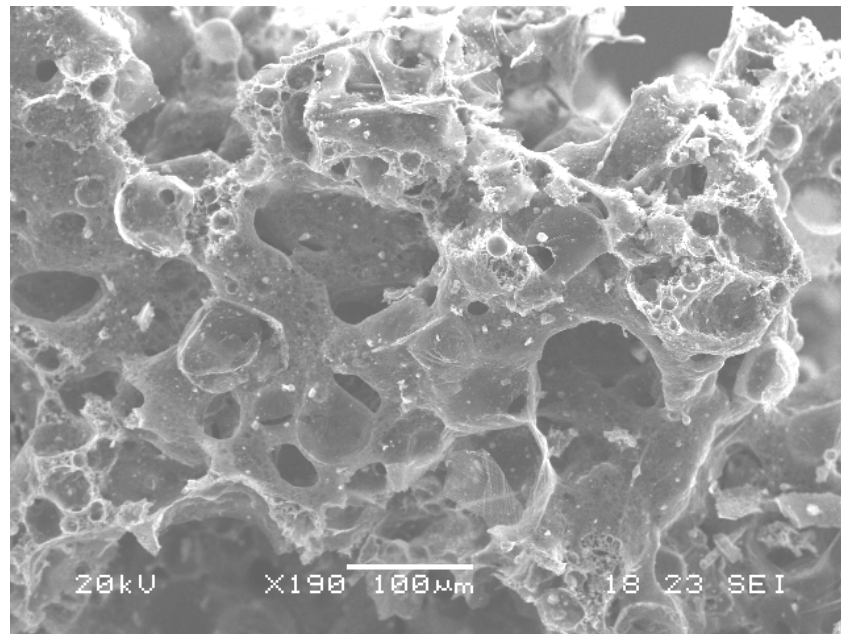


Figure 19 800°C-degraded sample

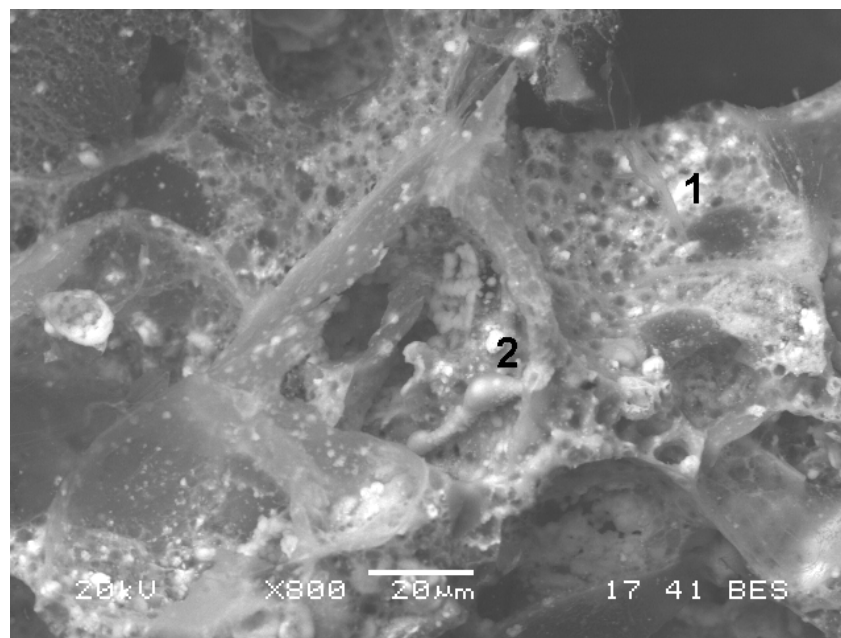


Figure 20 Particle magnification of a degraded sample

According to Figure 19, the degraded sample contains a high amount of pores. These are linked forming an open-pore structure. Table 13 reports the results of a composition analysis.

| | Virgin | Residue | Residue (rescaled) |
|--------------|---------------|----------------|---------------------------|
| C | 35.89 | 11.46 | 3.98 |
| O | 52.96 | 64.12 | 22.44 |
| Al | 0.48 | | |
| Si | 3.18 | 3.85 | 1.35 |
| P | 4.20 | 11.66 | 4.08 |
| Ca | 2.46 | 6.53 | 2.29 |
| Ti | 0.84 | 2.37 | 0.83 |
| Total | 100.00 | 100.00 | 34.97 |

Table 13 Composition analysis (%weight) of a degraded sample

Second column shows the average composition of the sample from Figure 19. The composition must be rescaled in order to compare it to the virgin composition, since the residue is a 35% of the original mass. Third column shows the result of rescaling operation. This way, first and third columns can be compared. As can be seen, there has been a drastic decrease of the carbon and oxygen amount, whilst the other elements maintain an approximately constant composition. This can be due to organic compounds and water loss mainly.

This behaviour is due to the fact that the filler does not chemically react and remain inside the sample also after burning at 800°C. According to Figure 20, point number 1 shows elements referred to the filler present in the virgin material, whilst point number 2 shows a composition similar to the calcium carbonate.

2.4.2. Vermiculite-cement coating: Fendolite™

Characterization of high temperature exposure behaviour in TGA tests

Interpretation of the TGA curve

Figure 21 reports a typical weight loss curve as obtained for a virgin Fendolite™ sample in a TGA test. The represented curves are the weight loss percentage and its derivative (%/°C) at 10°C/min:

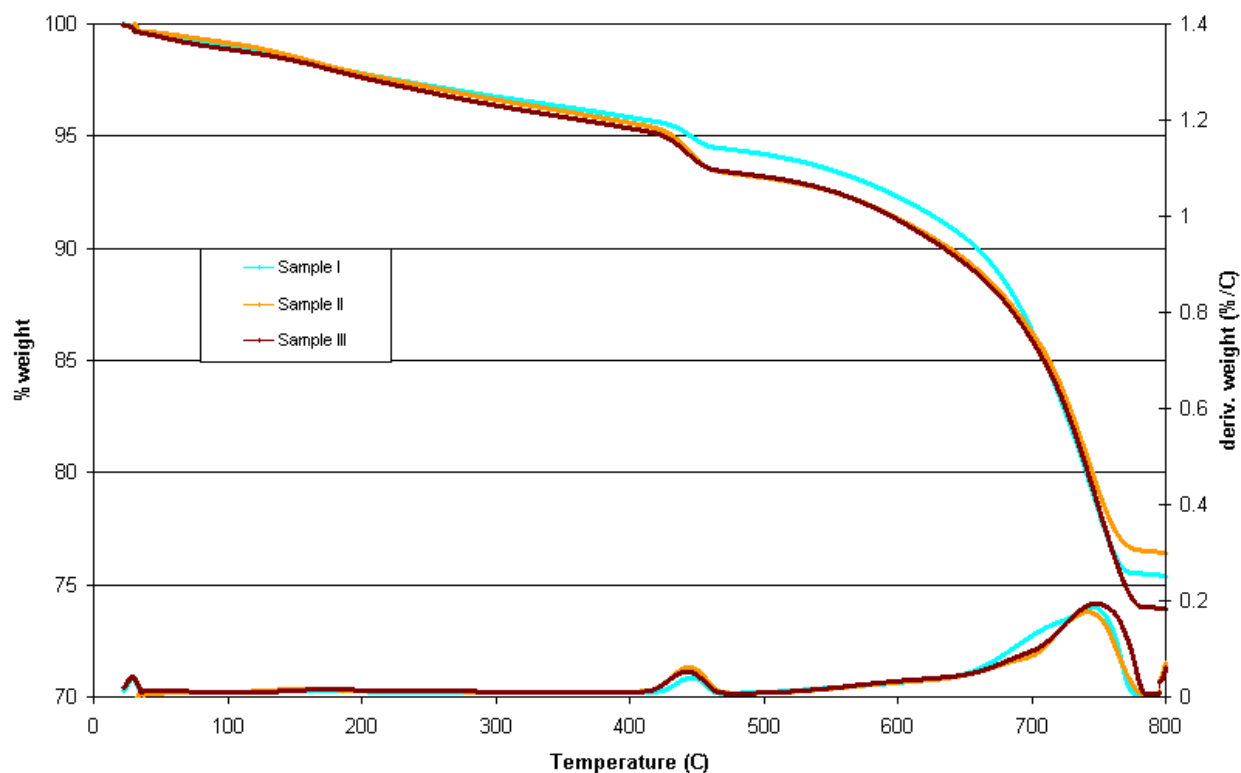


Figure 21 Virgin Fendolite samples at 10°C/min

There are three main regions where different phases take place (Figure 21):

1. First region: water loss.
2. Second region: dehydroxylation.
3. Third region: CO₂ loss from carbonization, i.e. decarbonation.

These phases can be recognized taking into account the derivative (%/°C) shift, i.e. when there is a peak, a new reaction is taking place. Moreover, the different regions are consistent with information found in literature. For example, according to the essay *Measurement methods of carbonation profiles in concrete: thermogravimetry, chemical analysis and gammadensimetry* (Villain et al., 2007) and *Physicochemical, mineralogical and morphological characteristics of concrete exposed to elevated*

temperatures (Handoo et al., 2001) it is known that there is a decarbonisation at 510-900°C. As can be seen, the major loss takes place during this phase.

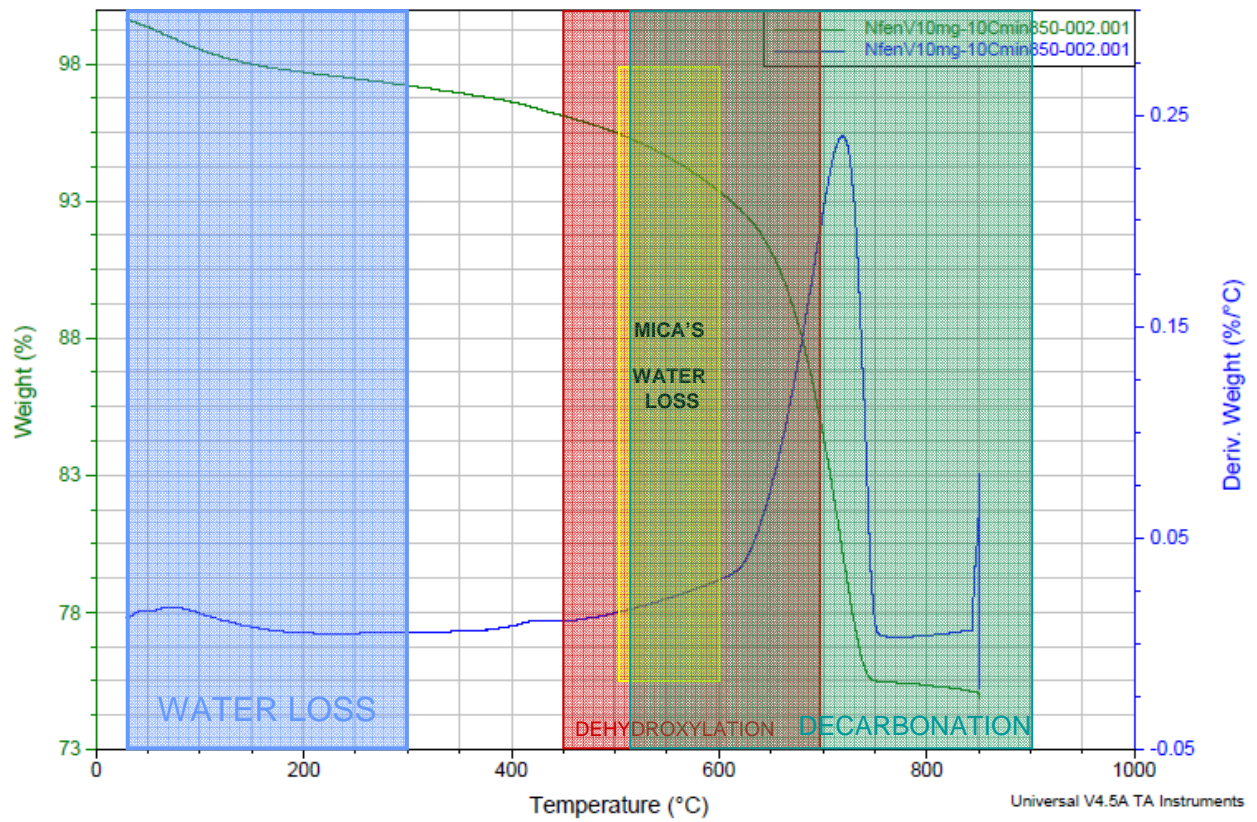


Figure 22 Virgin sample of Fendolite™ burned in the TG until 850°C

Source: Villain, Alarcon-Ruiz, Ptáček, Handoo

The curve shows a behaviour similar to one presented by limestone-concrete samples reported in the literature (Figure 23).

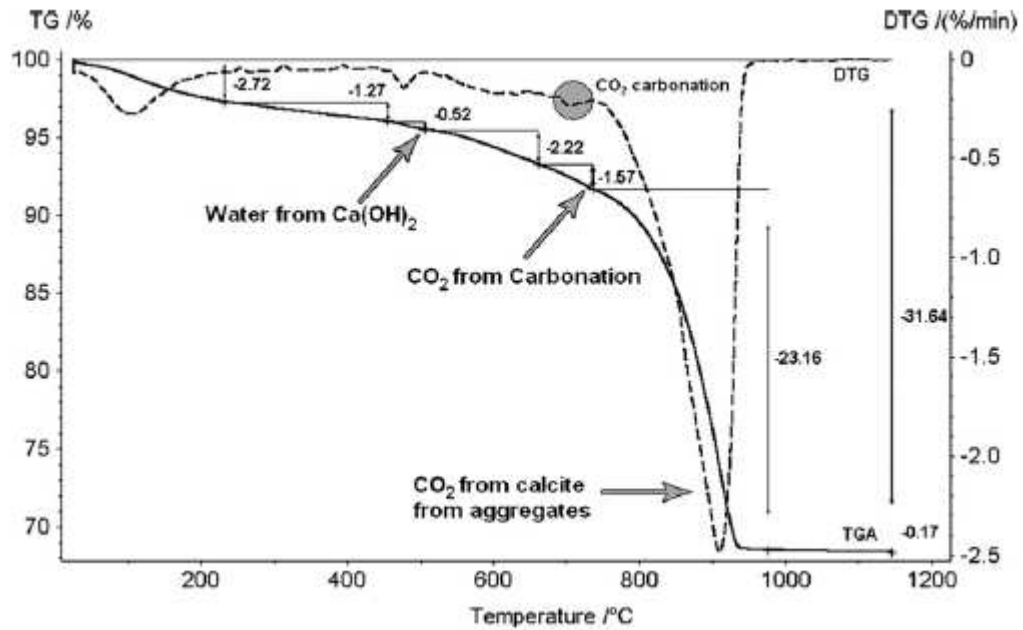


Figure 23 Dissociation of a carbonated sample of crushed concrete mortar during a TGA test: concrete containing limestone aggregates.

Source: Villain et al., 2007

The similarity can be explained by the high percentage of cement in Fendolite™ (30 to 60% mass). According to literature (Alarcon-Ruiz et al., 2004), a common cement contains:

- 59% CaO
- 19,45% SiO₂
- Other compounds

The components of cement are responsible of a great amount of CO₂ release during the decarbonisation phase.

A sample of common cement was analyzed in order to compare it to the Fendolite™ curve (Figure 23 24) In this way it could be observed that the Fendolite™ shows a similar behaviour to cement, thus it has a significant amount of this material. The differences found between the final losses, about almost 4%, are due to other components of the material. It has to be pointed out that cement losses water at 700-750°C.

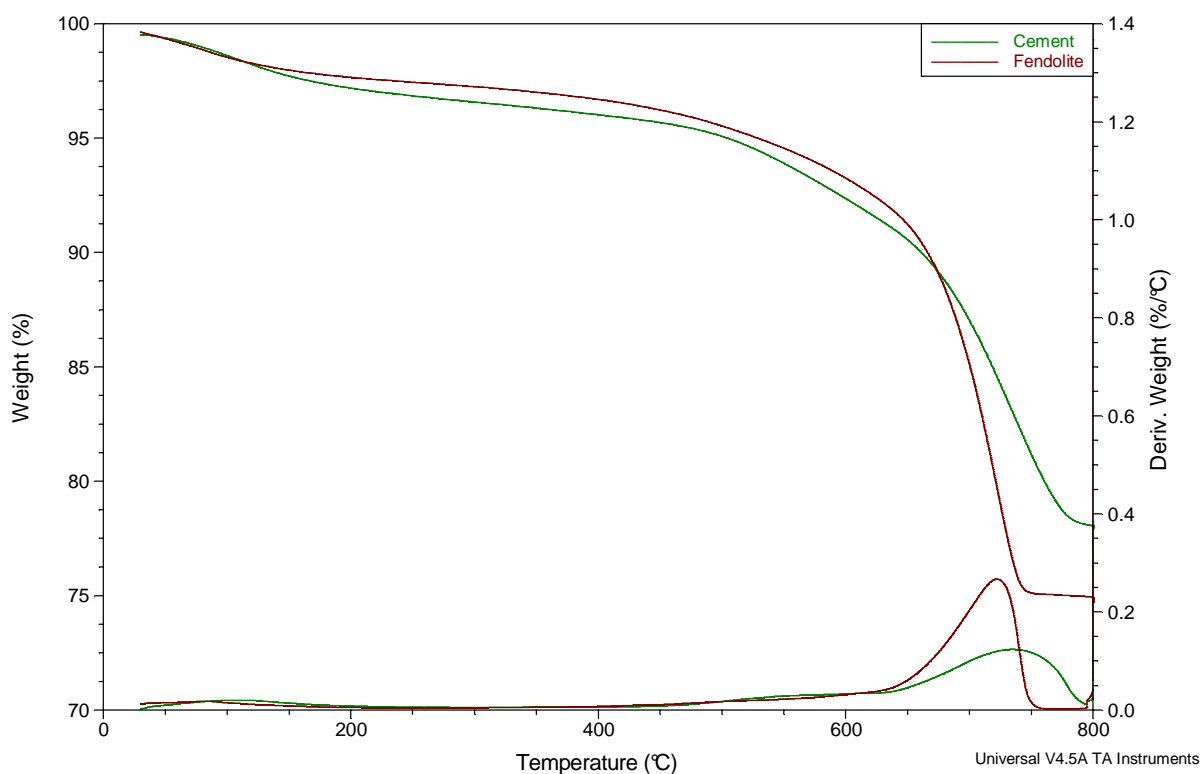


Figure 24 Cement versus Fendolite™

Figure 21 clearly shows an important weight loss concentrated at approximately 400°C, probably due to vermiculite (mica) degradation. To confirm this hypothesis, a mica sample was tested.

In order to obtain a mica sample, a piece of material was grinded to powder and vermiculite sheets were isolated.

Three TGA experiments were carried out. In Figure 25 is shown a comparison between pure mica and Fendolite™. This revealed that:

- Mica losses water at 400°C and 650°C, approximately (figure 12).
- Mica’s weight losses are low till 800°C. A test was carried out at higher temperature (950°C) in order to observe the complete material degradation.
- The contribution of mica to the peak at 700°C in Fendolite™ can be considered low. Cement is responsible of the greater amount of weight loss. The main release at this temperature could be CO₂.
- Obviously, Fendolite™ has a greater final loss than cement, because it contains more compounds that release gas.

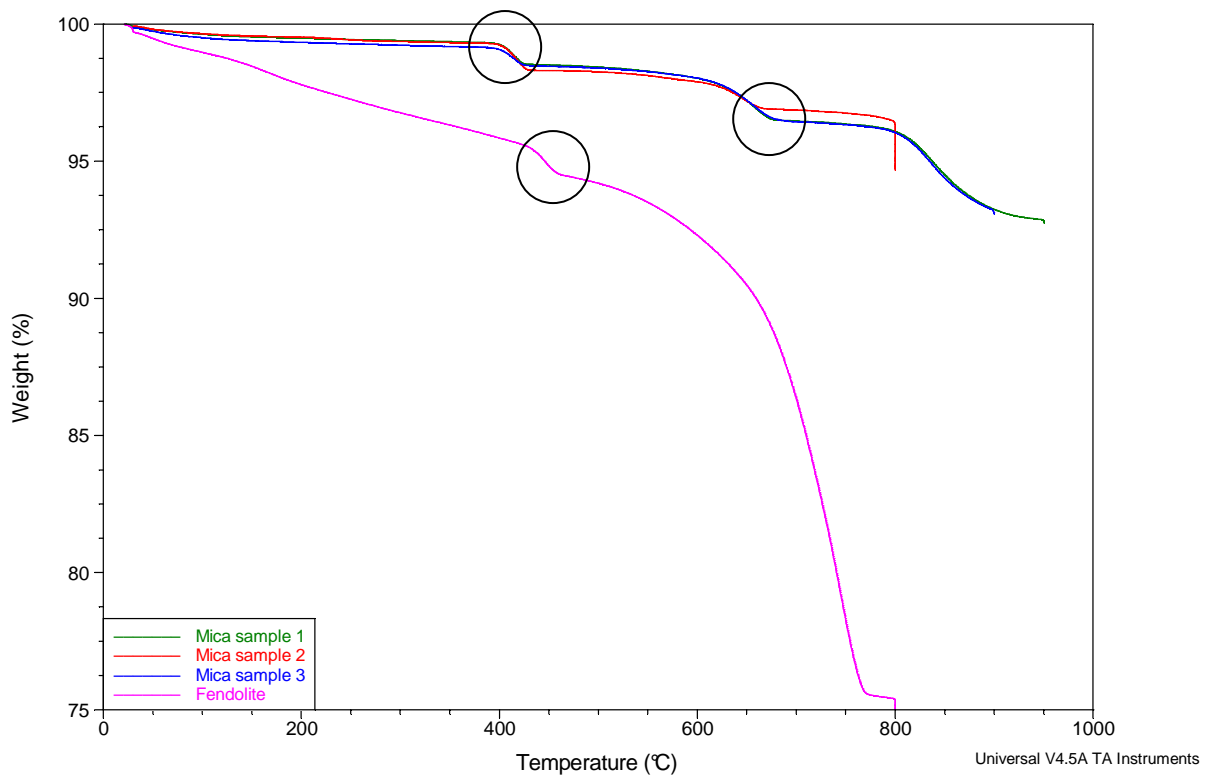


Figure 25 Mica tests versus Fendolite™

Analysis of re-hydrated samples

As discussed, major weight losses in the sample during TG tests were attributed to expulsion of water and of carbon dioxide. Specific tests were carried out to explore the possibility of the sample to re-integrate such component from the ambient air. In such, it must be intended an attempt of “validation” of the hypothesis reported above.

First, the samples were exposed to high temperatures reaching a maximum of 800°C with a heating ramp. Then, without opening the furnace, the tests were redone to ensure the total degradation of the compounds. After, the samples were kept in an container next to a little container with water. One sample was kept there for 24 hours. The other, for a week. Once re-hydrated, the samples were re-exposed to the same thermal treatment in order to know whether there had been water absorption. As expected, a higher concentration of water was captured by the sample during a week than during a day, being then necessary the pre-treatment of the sample in the oven, in order to eliminate the water absorbed from environment. In Figure 27 it can be seen the derivative in weight (%/°C) versus temperature of a virgin sample, a one-day re-hydrated sample and a one-week re-hydrated sample. It can be easily seen the different water absorption for each case.

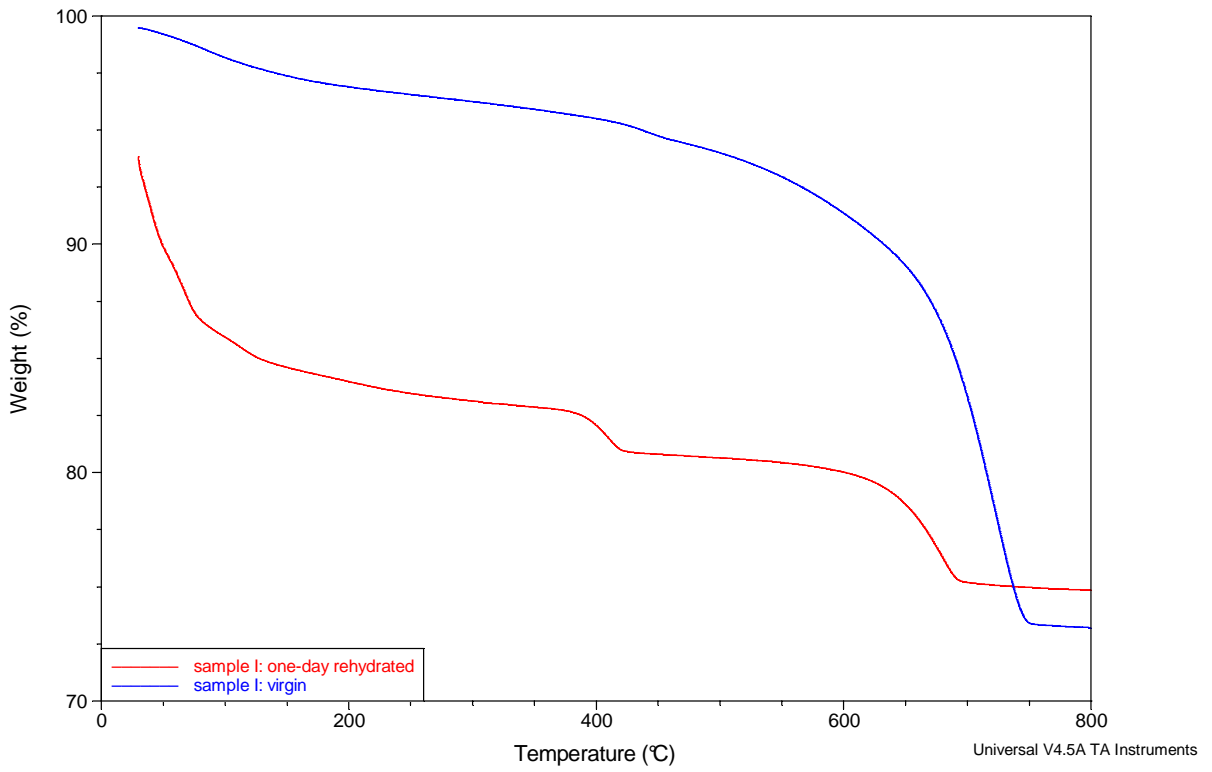


Figure 26 Percent weight for normal, one-week rehydrated and one-day rehydrated samples

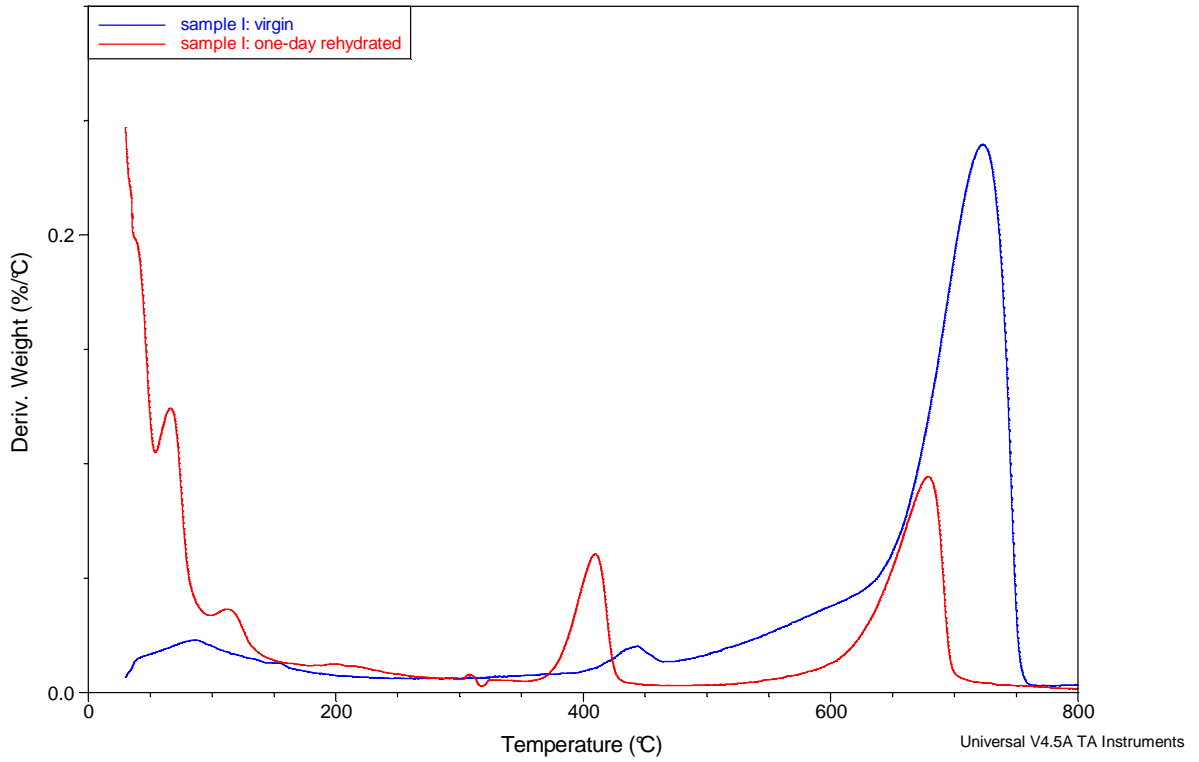


Figure 27 Temperature derivative of percent weight: virgin and one-day rehydrated

After carrying out several tests, it was noticed that the Fendolite™ curves rarely began at 100% in weight. That could be because of the water evaporation during the TG equilibration at 30°C. Moreover, the derivate showed initial irregularities until 100°C. That is why all the curves were re-scaled to begin with 100% weight at 100°C.

Characterization of high temperature exposure behaviour in Fixed Bed Tubular Reactor tests

Several tests were done using the tubular furnace in order to compare the results to those obtained in the TG, as well as to obtain samples to carry out other studies, such as SEM (Scanning Electron Microscope) analysis, densities of degraded material, etc.

The tests were done following the procedure described in section 2.2.2. The results were used to study the following items:

- *Weight measurement before and after degrading:*

The samples were weighted in order to calculate the percentage of weight loss after heating at different temperatures (250, 350, 500 and 800°C) in the furnace. The results were compared to those obtained from the TG (Figure 28). As can be seen, the tests from the oven did not exactly match the TG ones. However, the results were acceptable, specially at 250 and 800°C.

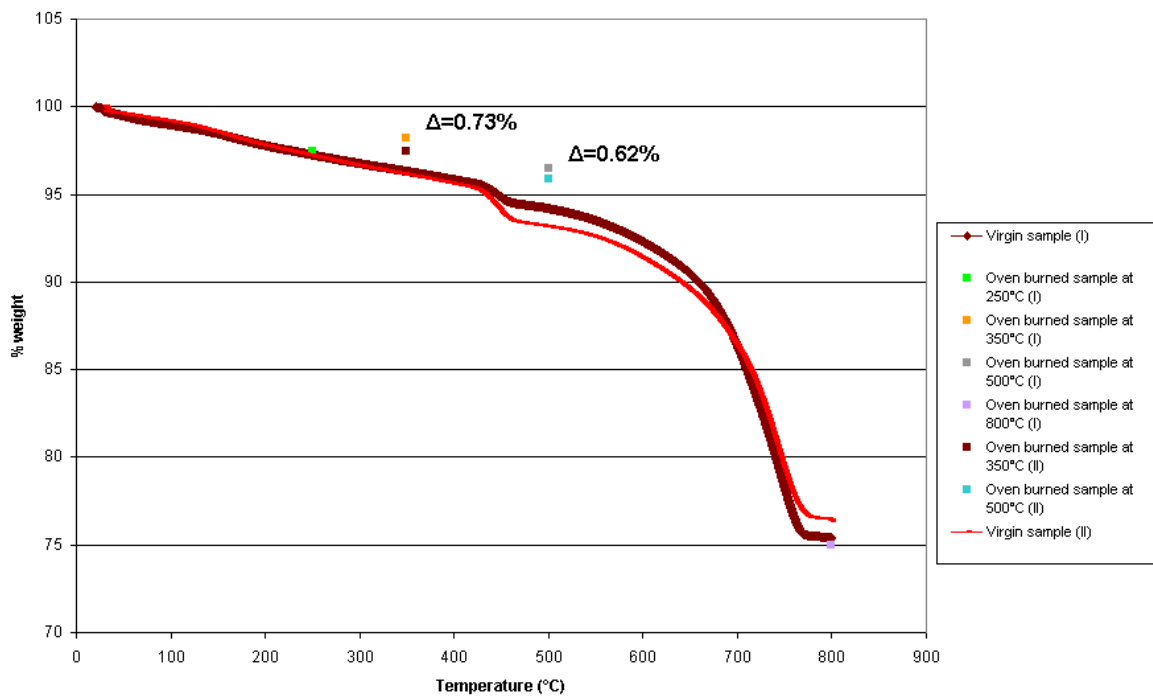


Figure 28 Comparison between oven and TG results

As can be seen, the difference between both tests at 350 and 500°C is lower than 1%, thus good reproducibility is experienced.

According to these tests the weight losses for critical regions of Fendolite™ degradation are:

| Region | Weight loss (% of weight of the conditioned sample) |
|---------------------|---|
| From 100°C to 350°C | 2.8 |
| From 350°C to 500°C | 2.9 |
| From 500°C to 800°C | 16.9 |

Table 14 Weight loss (%) at each region

– *Description and amount of product collected in the traps:*

Following the procedure of section 2.2.2., the gases from the tubular reactor were cooled and partially condensed in the traps. The amount of condensate was in general very low. In Figure 29, the percentages of condensable and non-condensable gases released from degradation were plotted. Percentage of non-condensable gases was calculated by difference between initial weight and final sample and condensate mass. There can be seen as the major condensate collection in traps occurs at 800°C, when most of the Fendolite™ compounds have been degraded. Condensable and non-condensable gases have very similar profile.

The product obtained in the traps is a transparent liquid which is likely to be water.

The region which refers to cement degradation (500-800°C) yields a greater amount of non-condensable gases, which are very likely to be CO₂. This confirms the information about cement from literature.

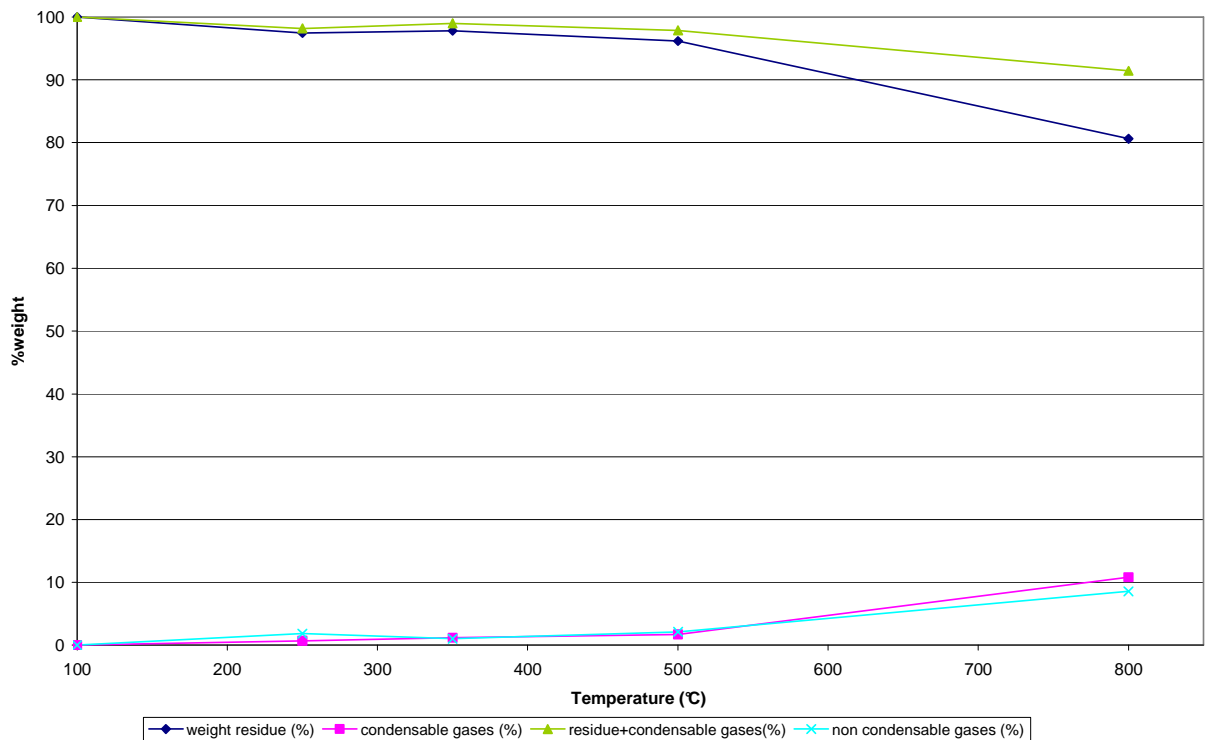


Figure 29 Oven tests at different temperatures: weight residue, condensable and non-condensable gases, residue plus products obtained from traps (%)

– *Density assessment before and after burning:*

A density evaluation was done before and after burning. Two different densities were obtained:

1. Real density:

A pycnometer (Figure 30) was used in order to obtain the real density. First, the sample was crunched to powder to eliminate as much as possible the pores. The pycnometer was weighted and then filled with xylene. It was introduced in the oven until achieving an established temperature of 26°C. Once achieved, the pycnometer with the xylene were weighed together. Then, the liquid was released and the pycnometer was dried. The sample powder was introduced and it was all weighted together. After, the recipient was filled with the xylene and the same process in oven was repeated. As the xylene density and the powder weight were known, the displaced liquid volume could be calculated, thus the real density obtained.



Figure 30 Empty pycnometer

The value of real density obtained was of $\rho_{real} = 2475 \text{ kg/m}^3$.

2. Apparent density:

The Archimede' principle was used in order to obtain the Fendolite™ apparent density. This density value considers all the pores inside the material. First, the samples were covered with paraffin to avoid the water filling the pores. Once recovered, the samples were immersed in water and the apparent density calculated from the difference of weight inside and outside water.

The value obtained was of $\rho_{apparent} = 530 \text{ kg/m}^3$.

This corresponds to a void percentage of:

$$\frac{\rho_{apparent}}{\rho_{real}} = \frac{530}{2475} = 0.214 \rightarrow void\% = (1 - 0.214) \cdot 100 = 78.6\%$$

Characterization of high temperature exposure behaviour from morphological analysis

A Scanning Electron Microscope was used in order to carry out morphological analysis of samples from Fixed Bed Tubular Reactor tests. Two different samples were studied: virgin and 800°C-degraded Fendolite™.

A preliminary analysis of the samples was conducted without the microscope. Figure 31 shows virgin pieces of material. Several pores and mica sheets can be seen.

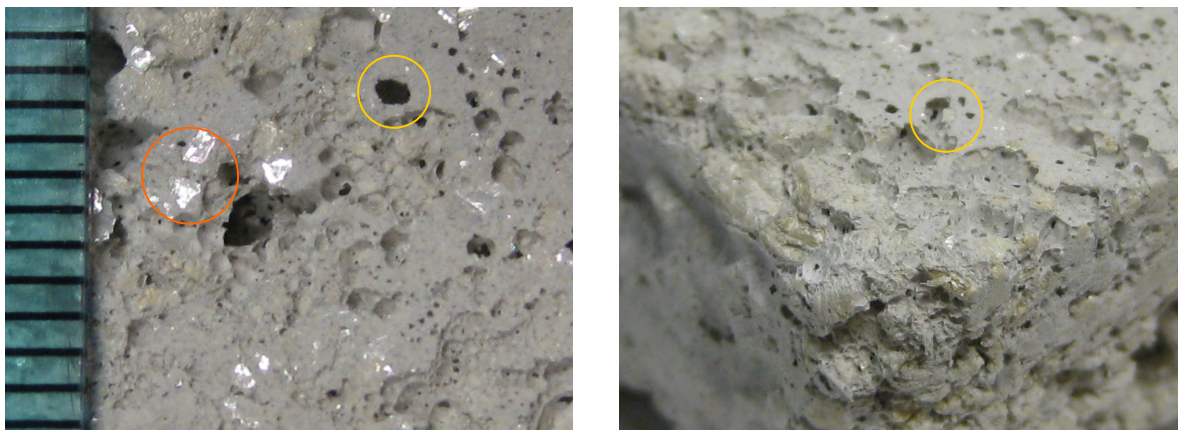


Figure 31 Fendolite™ with mica sheets and pores

As the information obtained was not enough, a SEM analysis was necessary to know the element composition and the pore dimension.

Virgin sample

Figure 32 shows the SEM image of a non-burned sample of Fendolite™. The mica sheets can be clearly seen. When focusing on them, the element percentages (Table 15) confirm that the sheets refer to vermiculite.

| | %Weight | |
|----|---------|--------|
| | Global | Sheets |
| C | 3.48 | - |
| O | 51.05 | 45.88 |
| Mg | 0.89 | 10.42 |
| Al | 2.26 | 6.00 |
| Si | 5.96 | 19.23 |
| S | 0.58 | - |
| K | 1.16 | 9.07 |
| Ca | 32.87 | 3.74 |
| Fe | 1.76 | 4.68 |
| Ti | - | 0.98 |

Table 15 Element composition of a virgin sample: global and mica sheet percentages

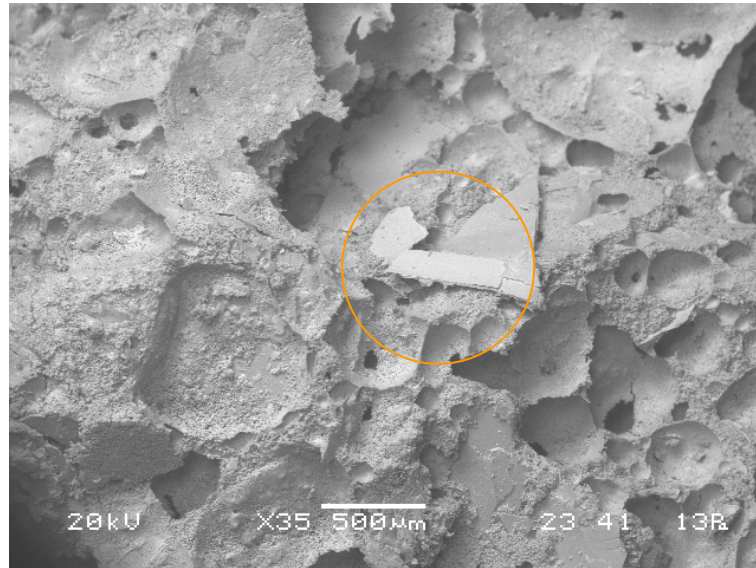


Figure 32 Virgin Fendolite™: mica sheets

As it can be seen, the pore structure is complex. Pores are communicating and voids constitute a significant fraction of the material. This is in good accordance with the void fraction calculated in section 2.4.2. The pore dimension can be calculated. From the figure, the diameter average value of macropores is approximately $\phi 460 \mu\text{m}$.

800°C-degraded sample

Figure 33 shows the SEM image of a 800°C-degraded sample of Fendolite™, where it can be observed that the material is more fractured, but qualitatively similar.

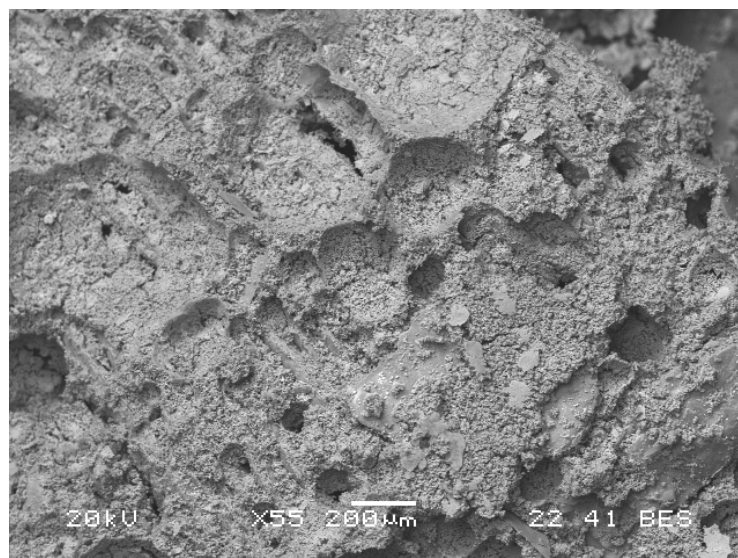


Figure 33 800°C-degraded Fendolite™

Comparison

Table 16 shows the element composition of virgin and degraded samples.

| | Virgin global | Mica sheets | 800°C-degraded |
|----|---------------|-------------|----------------|
| C | 3.48 | 0.00 | 0.00 |
| O | 51.05 | 45.88 | 30.81 |
| Mg | 0.89 | 10.42 | 0.59 |
| Al | 2.26 | 6.00 | 1.14 |
| Si | 5.96 | 19.23 | 5.07 |
| S | 0.58 | 0.00 | 0.50 |
| K | 1.16 | 9.07 | 0.32 |
| Ca | 32.87 | 3.74 | 36.17 |
| Fe | 1.76 | 4.68 | 1.62 |
| Ti | 0.00 | 0.98 | 0.00 |

Table 16 Virgin and degraded samples comparison

The values to be compared are those virgin global and 800°C-degraded rescaled. Several aspects must be pointed out:

- The carbon reduction is due to the carbonisation of the material and the formation of CO₂. This reinforces the information from literature and the material characterisation (section 2.3.2. and 2.4.2.).
- There can be seen a morphological change.

Differences in pore dimension could be due to random, since the material is heterogeneous.

2.5. Degradation kinetic modelling for Fendolite™

For Fendolite™, a kinetic apparent model was obtained in order to simulate its behaviour. In order to achieve this goal, first a set of tests were carried out to identify the degradation regions. Then, an apparent kinetic model was developed. Section 2.5.2. reports the results of the model.

2.5.1. TG tests used for the kinetic modelling

Definition of the sample form and weight

The preliminary step to kinetic modelling was the definition of an experimental protocol for collection of the kinetic data. A key issue was the definition of the sample form, intended as shape (chunk or powder) and weight.

- Sample form:

Initially, the tests were done using chunk samples since it is more similar to the real application form in industry. However, usual TG tests are carried out with powder samples, thus several tests were done in order to know whether the sample form affected the results. First, an amount of material was reduced to powder and was sieved at different particle sizes. A separation among phases was observed, obtaining a non homogeneous mixture. For this reason, the tests were redone pulverizing the material directly into the pan, disregarding the particle size. Moreover, several tests were carried out doubling the TG gas flow in order to see whether it affected the results.

In figure 34, there are the Arrhenius curves (see section 2.5.2) of samples burned at 5°C/min, for the case of chunk, powder and powder with double gas flow.

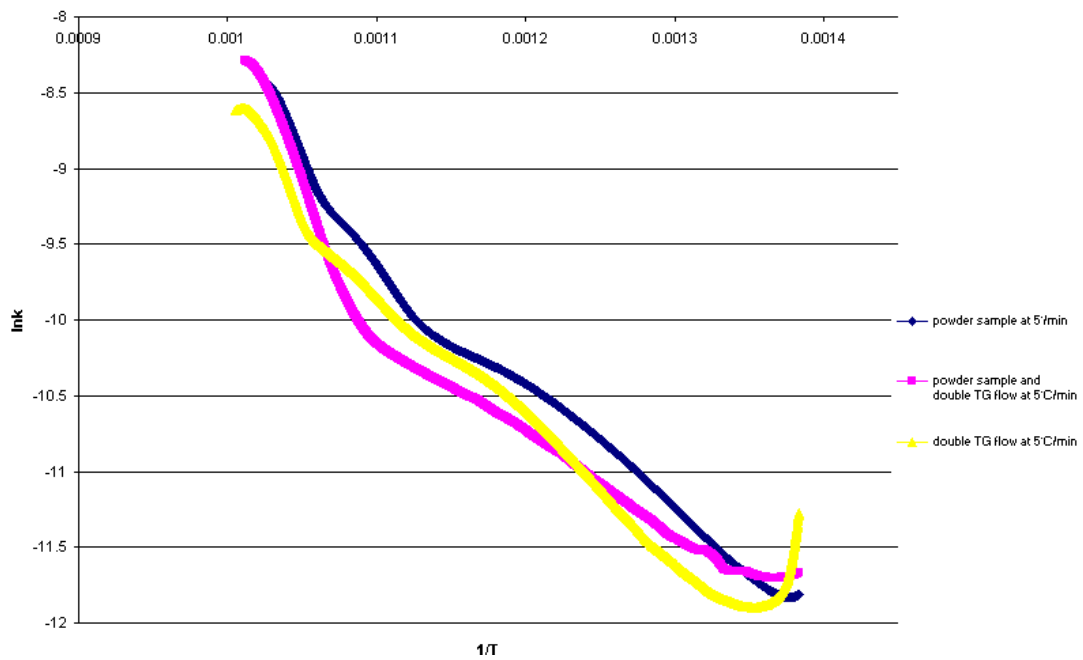


Figure 34 Arrhenius plot at 5°C/min: chunk, powder and powder with double TG gas flow

As can be seen, there is a negligible difference among the three tests. For these reason, and due to the difficulty in preparing the powder, it was decided to use chunk samples in the tests.

– Sample weight:

At the beginning, samples of about 10mg were used. Since the results were irregular, due to the heterogeneous material, it was decided to use 30mg-weight samples in order to have a representative sample with all the different components together, especially the mica sheets. A greater sample was not advisable since it may have introduced diffusion limitations.

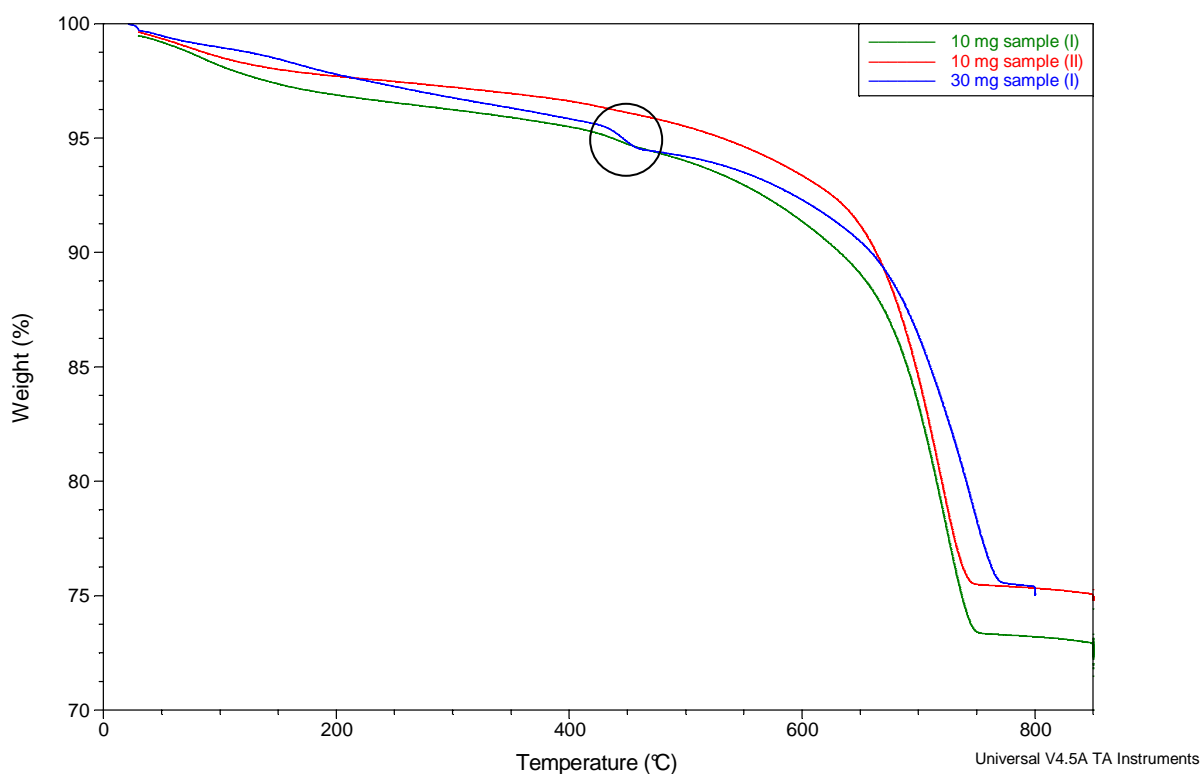


Figure 35 Sample weight comparison

As can be seen, in both 10 mg samples tested here there is no presence of the mica step, which it does appear in the 30 mg sample. The reason is that in smaller samples, there is a minor possibility of having significant quantities of mica due to their smaller size.

Results from the TG tests

In order to provide useful data for the development of the kinetic model, several tests have been performed. TGA tests were carried out for different heating rates: 5, 10, 25 and 45°C/min (figure 36). Greater rates were not possible due to technical limitations. Several repetitions for each heating rate were carried out. For some of them, final temperatures higher than 800°C were required to allow the process to finish. Before the beginning of the tests, the samples were conditioned in the oven to release initial moisture.

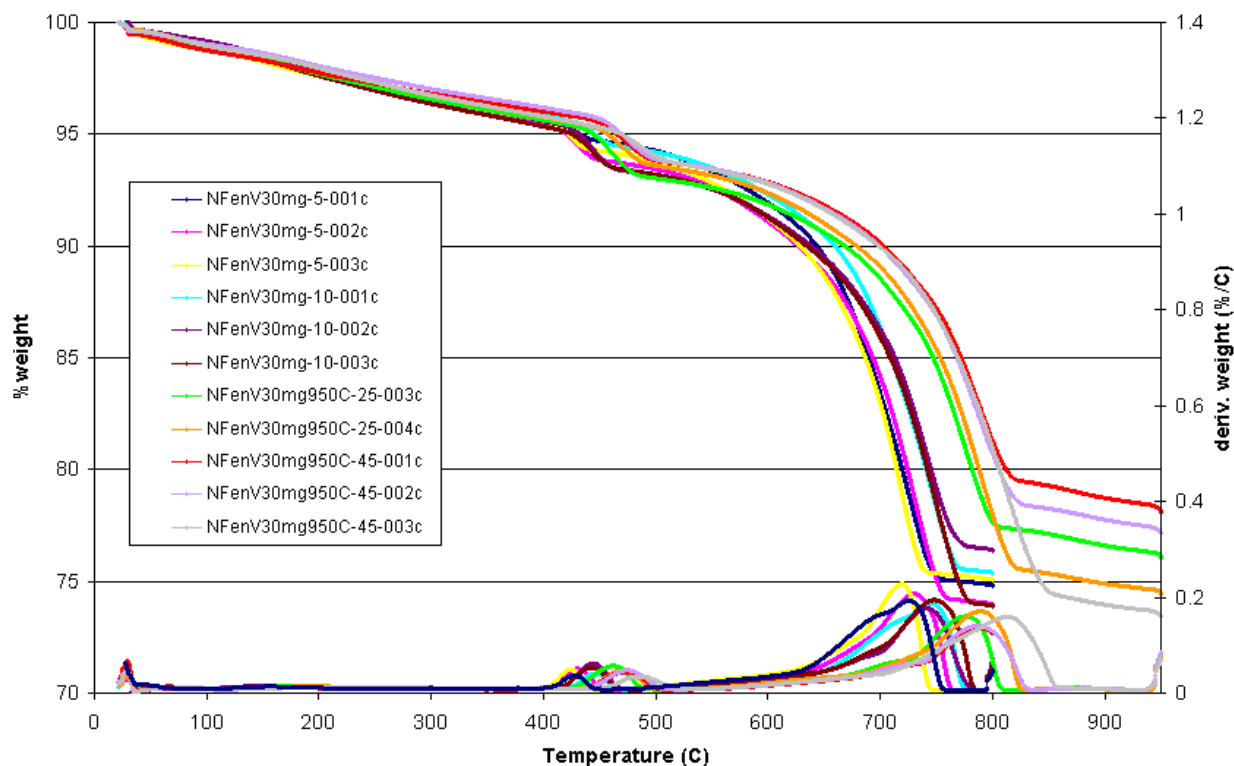


Figure 36 Experimental data obtained from the TG

As can be seen, the curves yield a different percentage of weight loss for each heating rate. Moreover, the finishing point is also different among the same set of tests.

When the heating rate increases, the curves are moved to the right, i.e. the reactions occur at higher temperature, and generally there is a lower final weight loss.

In the case of 25 and 45°C/min, the tests have to be carried out until 950°C in order to finish the reaction. All this variability is mainly due to heterogeneous characteristics of the material, as can be seen in figure 31.

Data treatment

It was seen the curves stabilized at 100°C, not being anymore influenced by initial humidity content of the sample, thus all the experimental data were rescaled in order to begin with 100% of weight at 100°C. As a result, all the curves started at the same point (Figure 37):

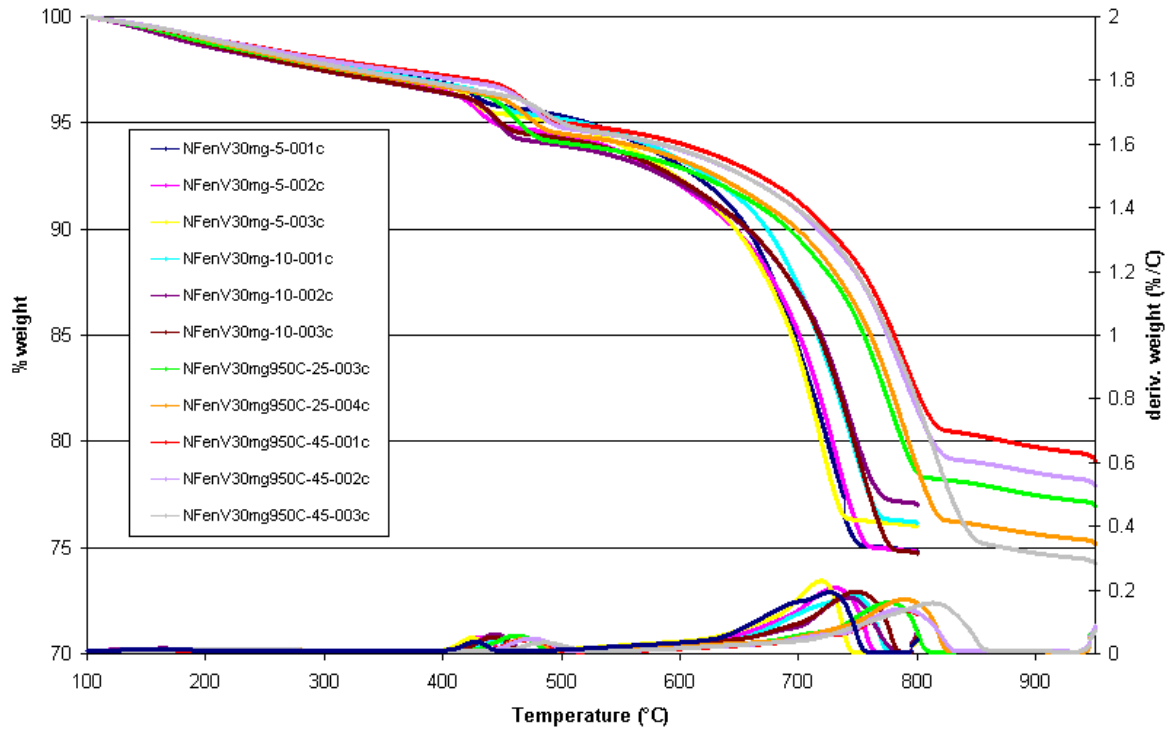


Figure 37 Rescaled experimental data

In order to rescale the data, all the values from 100°C onwards were calculated as:

$$\% w_{rescaled} = \frac{w}{w_{100^{\circ}C}} \cdot 100$$

Equation 5

Where w is the value at any point and $w_{100^{\circ}C}$ is the weight value at 100°C.

2.5.2. Development of an apparent kinetic model

The qualitative analysis of the TG weight loss curves clearly evidenced the existence of different degradation regions for the material (see section 2.4.2). This makes impossible the development of a kinetic model, although apparent, able to describe the for material degradation over the whole span from 30°C to 900°C with a single predictive equation.

Thus the temperature range was divided in 3 regions, for which specific apparent kinetic model were proposed. The mica's dehydration peak at about 400°C can be used to discriminate the three regions, roughly corresponding to the following temperature ranges:

1. Region I, before mica's peak: ~100-400°C
2. Region II, mica's peak: 400-450°C
3. Region III, after mica's peak: ~450-950°C

Region I

At low temperatures (below 100°C) water evaporation occur from the sample.

These water amount depends on environmental moisture and can be variable from one test to another, even though sample conditioning (see Appendix C) helps minimizing the effect.

Neglecting the moisture effect at low temperatures is conservative for fireproof modelling, thus it is neglected.

As could be seen in section 2.5.1., data were rescaled in order to start all the tests at the same temperature and neglect initial moisture. The resulting data are reported in Figure 37.

For Region I only a regression was used since an equilibrium-diffusion phenomenon took place instead of an Arrhenius degradation. All the data were plotted together and a lineal regression was made (Figure 38).

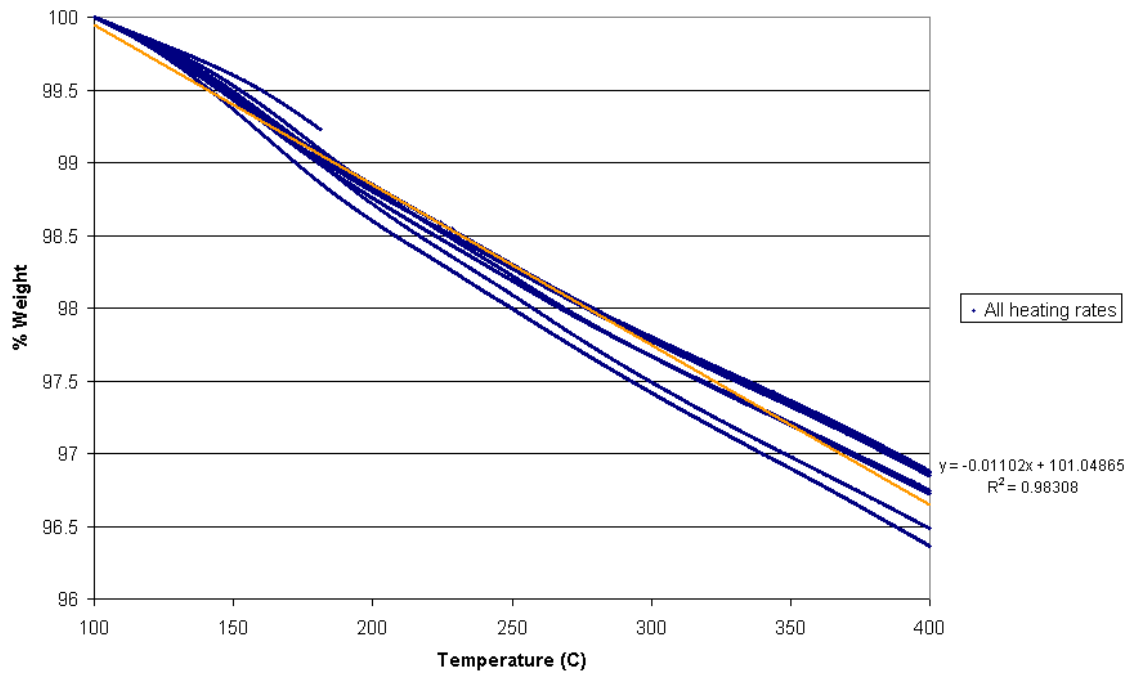


Figure 38 Region I: 100-400°C

Equation 6 shows the prediction equation for Region I, which is used for the simulation model. As can be seen, it is a simple model which only depends linearly on temperature.

$$\% \text{ weight} = -0,01102 \cdot T(C) + 101,04865$$

For $T < 400^\circ\text{C}$

Equation 6 Region I regression

Region II

For region II an Arrhenius model was proposed for describing the weight loss due to mica dehydration.

A mass conversion parameter was defined as the lost amount of mass at any time respect to total mass loss (ξ):

$$\xi = \frac{w_o - w}{w_o - w_f}$$

Equation 7 Mass conversion parameter

Where w_o and w_f are the weights at the beginning and the end of selected region.

The kinetic model has the generic form:

$$\frac{d\xi}{dt} = A \cdot e^{-\frac{E}{RT}} \cdot (1 - \xi)^m$$

Equation 8 Arrhenius equation

Where ξ is the mass conversion, A is the pre-exponential factor, E is the activation energy, R is the molar gas constant and m is the reaction order.

In order to obtain the model equation, first the derivative of weight with respect to time was calculated as follows:

$$\frac{dw}{dt} = \frac{d\%w}{dt} \cdot \frac{w_i}{100}$$

Equation 9

Where $\frac{d\%w}{dt}$ is obtained from the TG data and w_i is the initial sample weight at $t=0$.

Then, the derivative of conversion with respect to time is obtained from:

$$\frac{d\xi}{dt} = \frac{\frac{dw}{dt}}{w_o - w_f}$$

Equation 10

Figure 39 reports conversion and conversion derivative as a function of temperature:

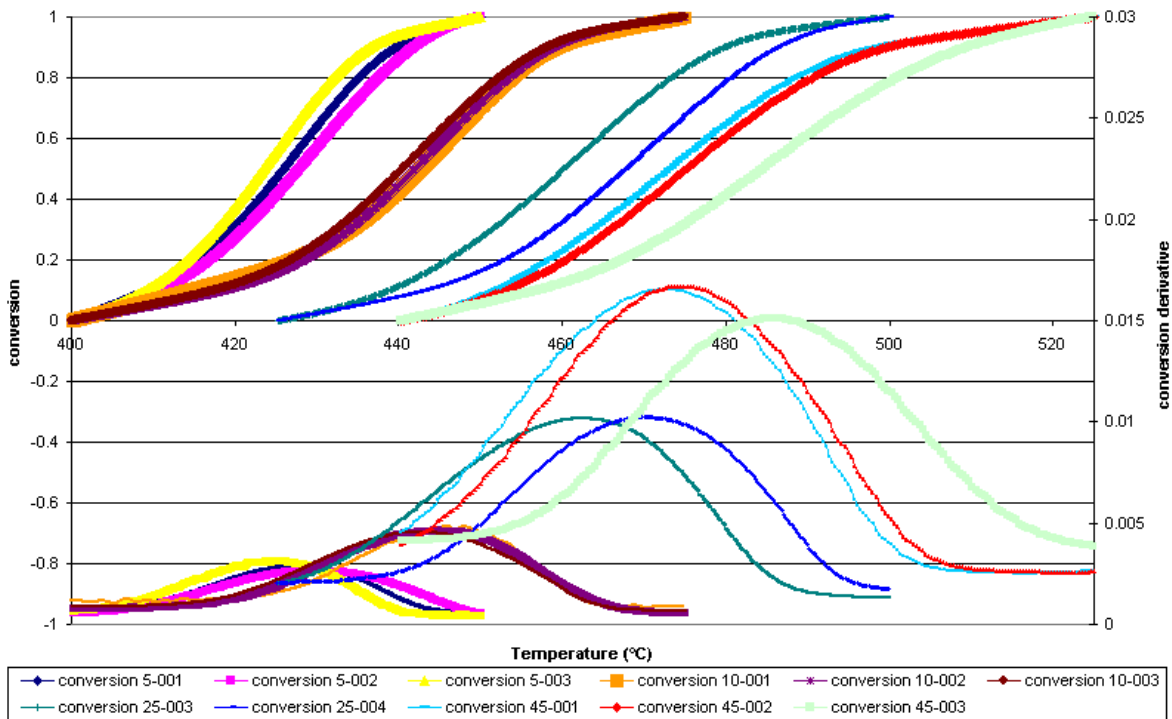


Figure 39 Conversion and conversion derivative

Obviously, when increasing the heating rate the variation of the conversion is faster.

Finally, the kinetic constant can be calculated using the next expression:

$$k = \frac{d\xi}{dt} (1 - \xi)^m$$

Equation 11

The next step is plotting $\ln k - 1/T(K)$. The reaction order (m) must be adjusted until the plot is a line. The best fitting for all the heating rates (i.e. 5, 10, 25 and 45 °C/min) yields the kinetic parameters (A and E) by regressing the equation:

$$\ln k = \ln A + \left(-\frac{E}{R}\right) \cdot \frac{1}{T(K)}$$

Equation 12

The range was represented by an Arrhenius model. First, the reaction order was modified until obtaining a line. The result was $m=1$. Figure 40 shows the Arrhenius plot obtained.

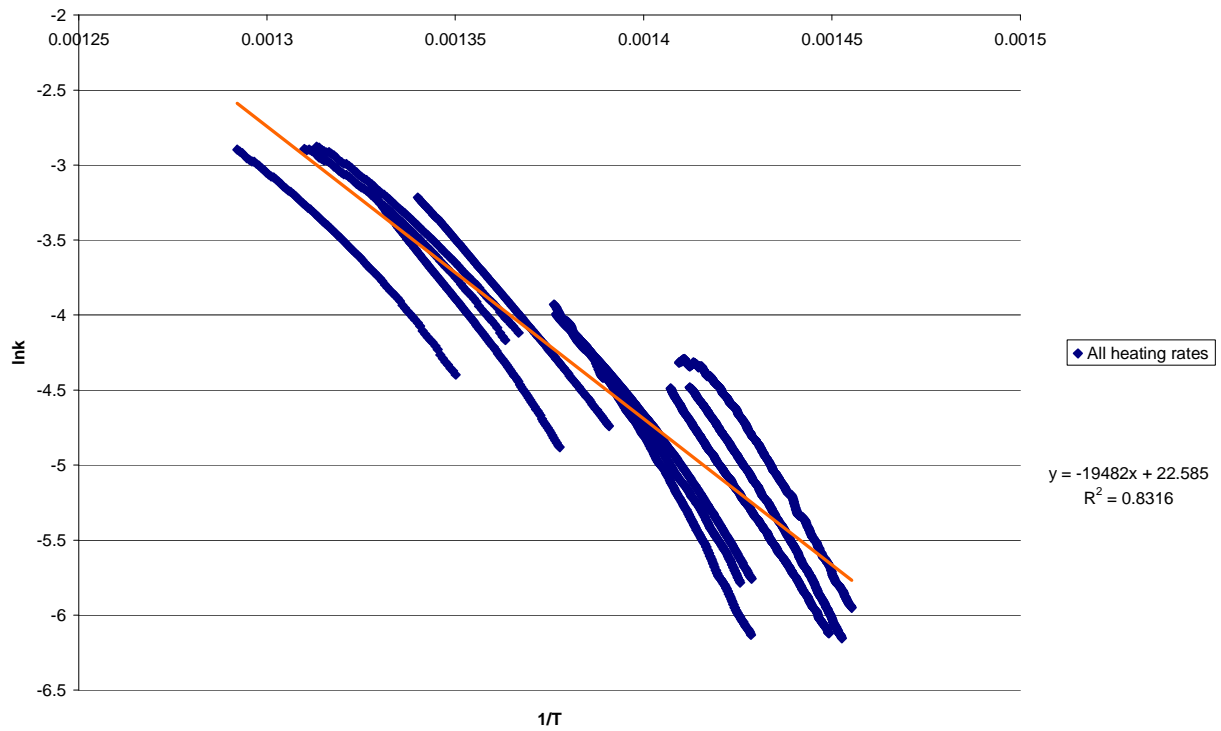


Figure 40 Region II before modifications

As the regression R^2 was not good enough and every heating rate yield a different slope, a solution was proposed. All the lines were moved to the right until had the same origin in the X axe. Then a filter for diminish the number of points was proposed. The final regression was thus:

$$\ln k = 43.975 + (-35013) \cdot \frac{1}{T(K)}$$

Equation 13 Regression equation for Region II

From this regression, parameters of kinetic equation can be calculated:

$$A = 1.25 \cdot 10^{19}$$

$$E = 290,958.03$$

And the kinetic equation is:

$$\frac{d\xi}{dt} = 1.25 \cdot 10^{19} \cdot e^{-\frac{290,958.03}{8.31T}} \cdot (1 - \xi)$$

A simulation at each heating rate was done (see *Demonstration of the kinetic model for global simulation*):

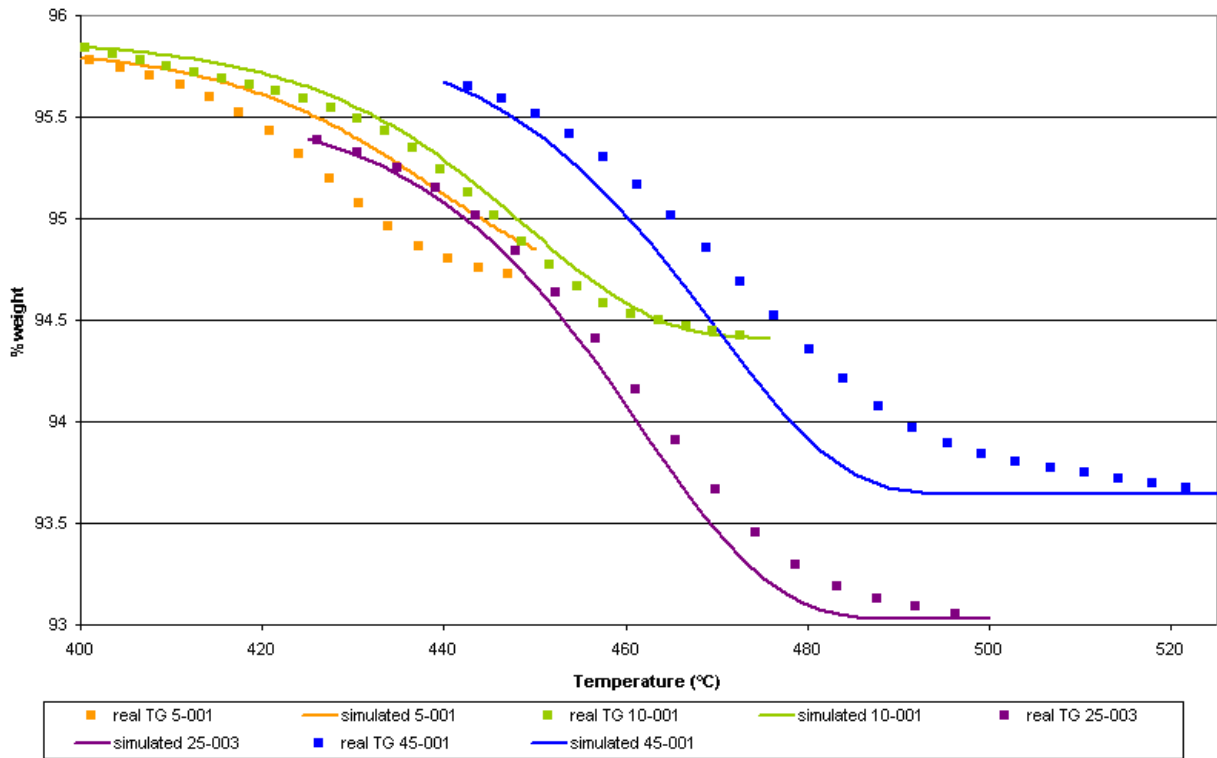


Figure 41 Simulation of Region II

As can be seen, the prediction does not match perfectly the real data. However, the error is acceptable. The best results occur at 10 and 25°C/min.

Region III

In Region III the same procedure followed for Region II was adopted. Figure 42 reports conversion and conversion derivative as a function of temperature:

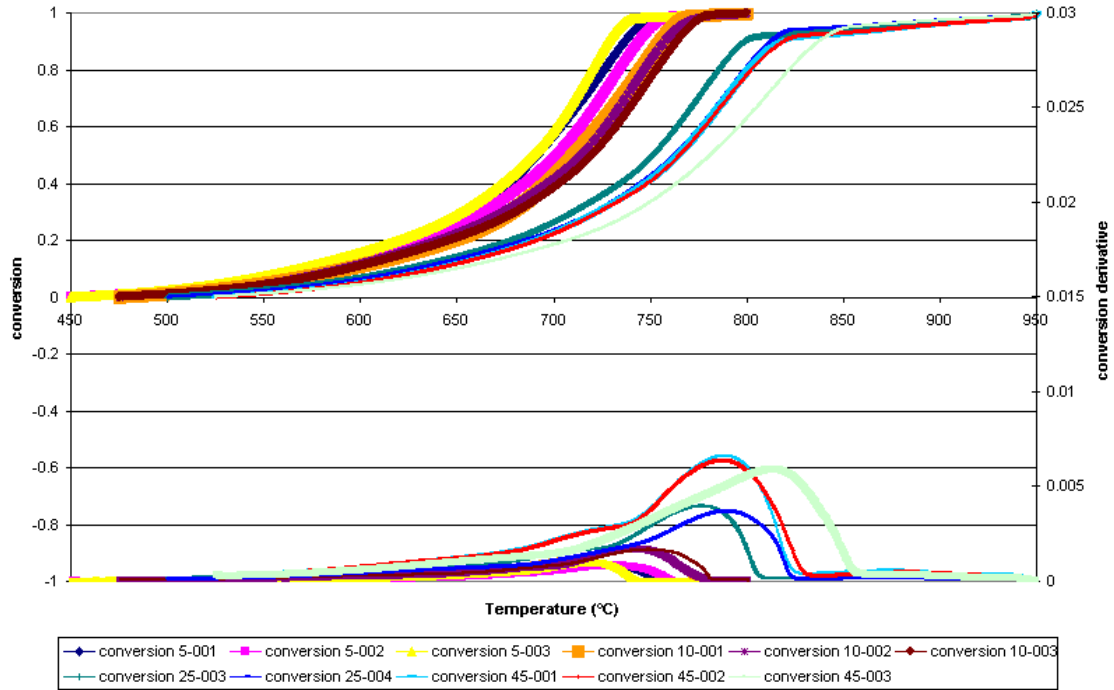


Figure 42 Conversion and conversion derivative

The range was represented by an Arrhenius model. The reaction order was assumed $m=0$. Figure 43 shows the Arrhenius plot obtained. A filter for diminish the number of points was applied for data representation in the figure.

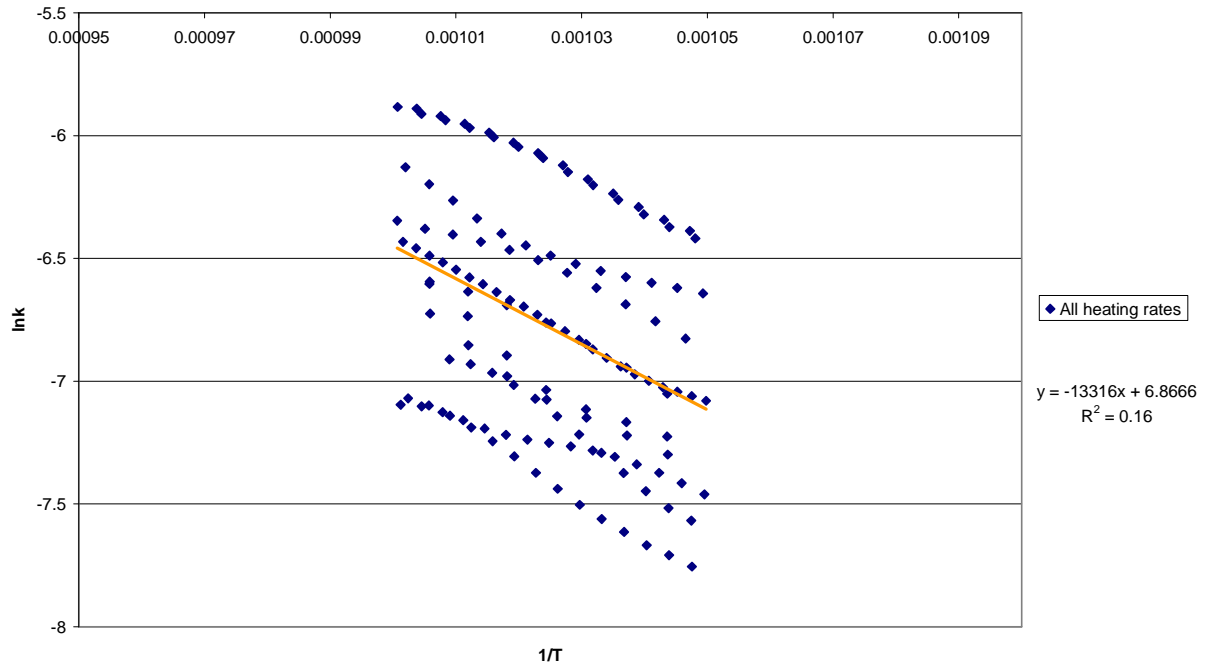


Figure 43 Region III

The final regression was:

$$\ln k = 6.8666 + (-13316) \cdot \frac{1}{T(K)}$$

Equation 14 Arrhenius equation for Region II

From this regression, parameters of kinetic equation can be calculated:

$$A = 959.68$$

$$E = 110,715.51$$

And the kinetic equation is:

$$\frac{d\xi}{dt} = 959.68 \cdot e^{-\frac{110,715.51}{8.31T}}$$

Figure 44 shows a simulation of Region III at each heating rate:

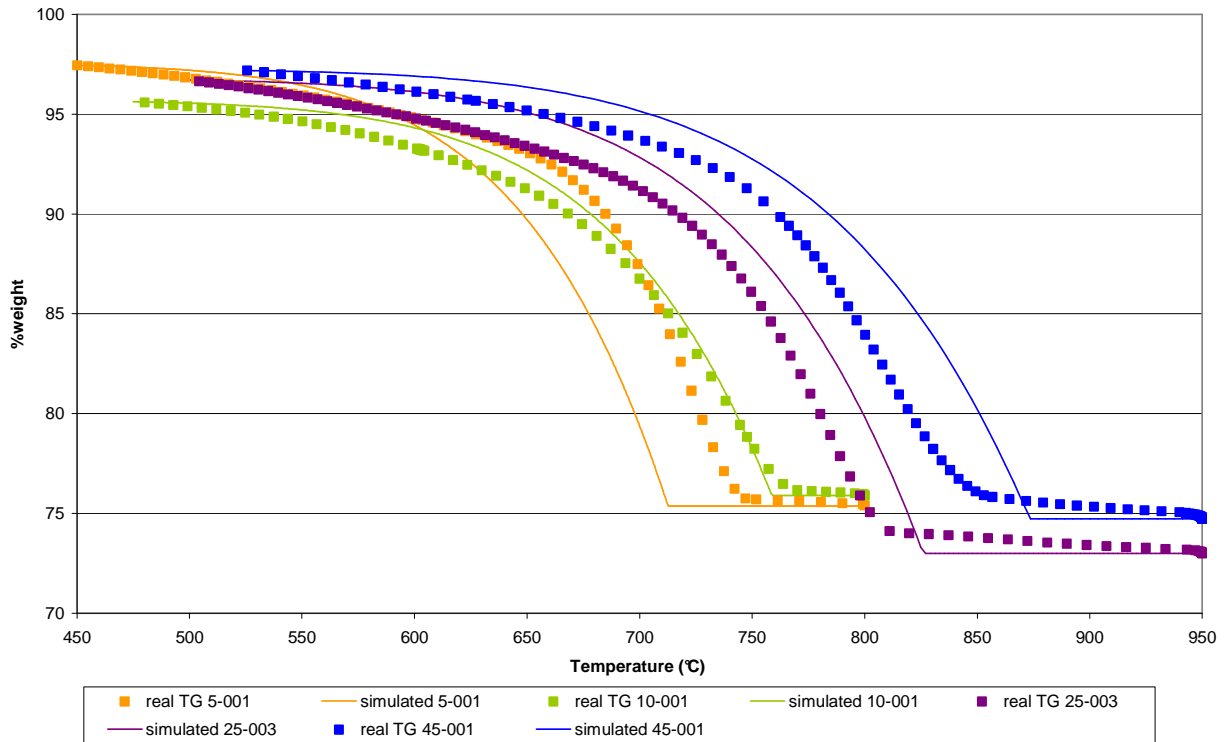


Figure 44 Simulation of Region III

Summary of the kinetic model

Table 17 summarizes the kinetic equations at each region:

| | Range | Kinetic Equation | Parameters |
|------------|------------|---|-------------------------------|
| Region I | ~100-400°C | $\% weight = -0,01102 \cdot T(C) + 101,04865$ for $T < 400^\circ C$ | $(W_0 - W_f) / W_0 = 3.37\%$ |
| Region II | ~400-450°C | $\frac{d\xi}{dt} = 1.25 \cdot 10^{19} \cdot e^{-\frac{290,958.03}{8.317T}} \cdot (1 - \xi)$ | $(W_0 - W_f) / W_0 = 1.8\%$ |
| Region III | ~450-950°C | $\frac{d\xi}{dt} = 959.68 \cdot e^{-\frac{110,715.51}{8.317T}}$ | $(W_0 - W_f) / W_0 = 19.49\%$ |

Table 17 Equation summary

Demonstration of the kinetic model

Since each curve finished in a different point, a new rescalation was done in order to better compare the data ¡Error! No se encuentra el origen de la referencia.. It consisted in an interpolation of all the data points in order to begin the curves at 100% in weight and finish at an average %weight calculated from all obtained data. The average residue was:

$$\% w = 76,9\%$$

The new plots were calculated by:

$$\frac{100 - 76,9}{w_o - w_f} = \frac{100 - x}{w_o - w}$$

Where w_o , w_f and w are the sample weights at the beginning, end and the current point, respectively. The x value corresponds to the %weight of the current point which is being recalculated.

Once the rescalation has been done, a simulation with the obtained equations was carried out.

The results were plotted together with the real data from the TG in order to demonstrate the reproducibility of the model.

Figure 45 shows the comparison between real and simulated data for the different heating rates.

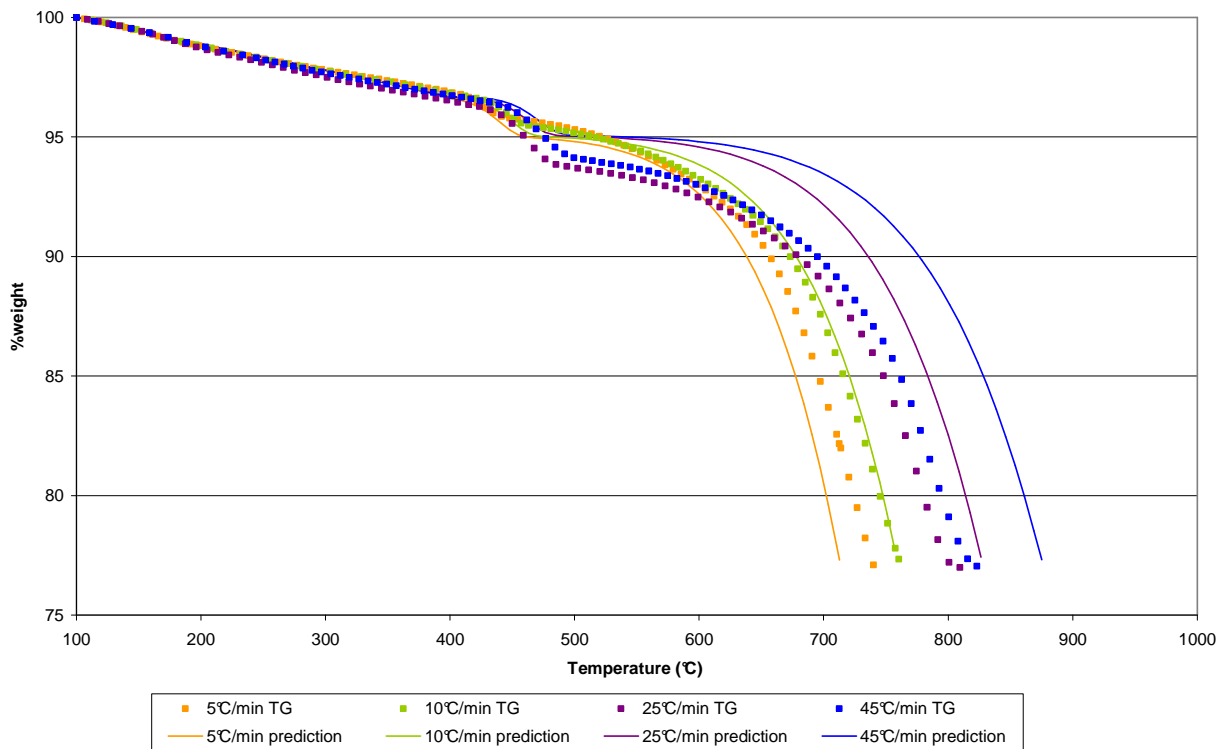


Figure 45 Prediction for different heating rates

3. CONCLUSIONS

In the present work, two different passive fire protection materials were studied and their behaviour at high temperatures was analysed. These materials consisted of an epoxy resin based material called Chartek7™ and a vermiculite-based cement coating commercially known as Fendolite™. Both morphological and physical properties were analysed for each material by laboratory scale tests (TGA, tubular furnace reactor, SEM, etc.). For the Fendolite™, an apparent degradation model was developed which could be used as input for further applications as finite element simulations of fire engulfment of process equipment.

The thermo-gravimetric tests evidenced three decomposition regions for Fendolite™:

1. Evaporative release (~100-400°C)
2. Mica dehydration (~400-450°C)
3. Cement dehydration and calcination (~450-950°C)

The similitude between Fendolite™ and a carbon-based cement was observed both in literature and carrying out thermogravimetric tests.

From the TG tests, an average final weight was determined at about 750°C, this temperature varying depending on the heating rate. The residue value was of a 76,9% of the initial sample weight.

Fendolite™ resulted very sensitive to ambient moisture, absorbing water when it was exposed to the environment. That is why it was necessary to pre-treat the samples and the results varied depending on the time of moisture exposure.

Parallel to thermogravimetric tests, several tubular fixed bed reactor experiments were carried out. The results were coherent with the TGA ones, thus confirming that the material behaviour was not affected by the scale of the tests. During the experiments, the amounts of condensable residue were monitored revealing that Fendolite™ apparently released water when exposed to heat.

In order to determine the morphological properties, a SEM analysis was carried out, showing the main components as well as the structural changes after the thermal degradation process.

For Fendolite™ the vermiculite sheets were observed. This analysis, also allowed to estimate the pores size and to observe the change of morphology of degraded and non degraded material.

In addition, apparent and real densities were determined experimentally for non degraded Fendolite™.

The values obtained were: $\rho_{real} = 2475 \text{ kg/m}^3$ and $\rho_{apparent} = 530 \text{ kg/m}^3$.

The void fraction was also calculated and equal to 78.6%.

An apparent kinetic model was developed from TGA test data, compiling three equations referred to the regions degradation above mentioned:

1. 1st degradation region (~100-400°C): modelled as a simple correlation since it corresponded to an equilibrium/diffusion phenomenon.
2. 2nd degradation region (~400-450°C): modelled as an Arrhenius apparent kinetics of first order.
3. 3rd degradation region (~450-950°C): modelled as an Arrhenius apparent kinetics of zero order.

The result fitted better the low heating rates, i.e. 5 and 10°C/min, while for 25 and 45°C/min the prediction did not represent exactly the real data. The more irregular results were those at the third region.

Dealing with Chartek7, an analogue thermal procedure was followed. Unlike Fendolite™, a final constant residue after exposure to high temperatures in the TG (800°C) was determined. The value was the 65% of the initial sample weight.

The Weight losses as a function of temperature observed at the TG were the same than the ones found during the tubular fixed-bed reactor tests. The residue was always about 35% of the initial weight.

The ratio of liquid residue formed during the Chartek7™ degradation was also analysed. Two types of liquid residue were captured: a transparent inorganic phase and a black organic phase. The organic fraction was obtained at temperatures higher than 400°C, while the other one, at lower temperatures.

SEM images for Chartek7™ showed some components which could be clearly distinguished: boric acid, APP and sand. It was also possible to observe that after the degradation process some pores were opened by the gas released (swelling phenomenon).

Considering all these results, some recommendations can be done. It is suggested to carry out further analysis of Fendolite™ in order to improve the apparent kinetic model.

Regarding to Chartek7™, since the differences observed at the SEM analysis and the high weight losses observed between the non degraded and degraded material, a deeper analysis of the char is advised.

4. BIBLIOGRAPHY

- Alarcon-Ruiz, L., Platret G., Massieu E., Ehrlicher A.: *The use of thermal analysis in assessing the effect of temperature on a cement paste*. June, 2004.
- American Petroleum Institute: *API14G-2007 Recommended Practice for Fire Prevention and Control on Fixed Open-type Offshore Production Platforms*. API Recommended Practice 14g Fourth Edition, April 2007.
- American Petroleum Institute: *API 2218-1999 Fireproofing Practices in Petroleum and Petrochemical Processing Plants*. API PUBLICATION 2218. Second Edition. August 1999.
- American Petroleum Institute: *API 2FB -2006 Recommended Practice for the Design of Offshore Facilities Against Fire and Blast Loading*. API Recommended Practice 2FB First Edition, April 2006.
- American Petroleum Institute: *API 2510-2001 Design and Construction of LPG Installations*. Api Standard 2510 Eighth Edition, May 2001.
- American Petroleum Institute: *API 2510A-1996 Fire-Protection Considerations for the Design and Operation of Liquefied Petroleum Gas (LPG) Storage Facilities*. API Publication 2510a Second Edition, December 1996.
- Casal, J.; Montiel, H.; Planas, E.; Vilchez, J.A.: *Análisis del riesgo en instalaciones industriales*. Edicions UPC, Barcelona, 1999.
- Center for Chemical Process Safety (CCPS): *Guidelines for Fire protection in chemical, Petrochemical, and Hydrocarbonprocessing facilities*. AIChE. New York, 2003
- Chartek7 material data sheet
- Cozzani V., Gubinelli G., Antonioni G., Spadoni G., Zanelli S.: *The assessment of risk caused by domino effect in quantitative area risk analysis*. August, 2005.
- DET NORSKE VERITAS (DNV): *Offshore Standard DNV-OS-D301 Fire protection*. 2008
- Droste,1992 (Lees): *Fire protection of LPG tanks with thin sublimation and intumescent coating*. *FireTechnol.*, 28, 257. 1992.
- Feldman, (Lees): *Subliming coatings for fireproofing of steel*. *Loss Prevention*, 8, 65. 1974.
- Fendolite material data sheet: CAFCO FENDOLITE M-II Brochure
- Gomez Mares, M.: *Chartek7 analysis*. 2010..
- Handoo S.K., Agarwal S., Agarwal S.K.: *Physicochemical, mineralogical and morphological characteristics of concrete exposed to elevated temperatures*. November, 2001.

- International Standard ISO 13702-1999: *Petroleum and natural gas industries - Control and mitigation of fires and explosions on offshore production installations - Requirements and guidelines*. First edition 1999-03-15.
- Jimenez M., Duquesne S., Bourbigot S.: *Characterization of the performance of an intumescent fire protective coating*. January, 2006.
- Jimenez M., Duquesne S., Bourbigot S.: *Intumescent fire protective coating: Toward a better understanding of their mechanism of action*. July, 2006.
- Jimenez M., Duquesne S., Bourbigot S.: *Kinetic analysis of the thermal degradation of an epoxy-based intumescent coating*. August, 2008.
- Kawaller: *Chemically reactive coatings for the protection of structural steel*. Fire Surveyor, 9(4), 36. 1980.
- Kayser, J.N.: *Testing fireproofing for structural steel*. Loss Prevention, 8, 45. 1974.
- Larcher S., Landucci G., Tugnoli A., Cozzani V.: *Experimental and numerical investigation of passive fire protection for pressurized tanks engulfed by fires*.
- Mannan, Sam, Lees: *Loss Prevention in the Process*. Third edition. Elsevier Butterworth-Heinemann. Oxford, UK, 2005
- MicroTech Sciences Limited: *How the SEM works*. 2007. Web site: <http://www.microtechsciences.com/how-the-sem-works.php>
- Muccini, Marco: *Analisi delle prestazioni di materiali per la protezione di apparecchiature da incendio esterno*.
- Muñoz, M. A.: *Estudio de los parámetros que intervienen en la modelización de los efectos de grandes incendios de hidrocarburo: geometría y radiación térmica de la llama*. Doctoral thesis. Departament d'Enginyeria Química. Universitat Politècnica de Catalunya. Barcelona, 2005.
- Norma Italiana UNI 10898-1-2001: *Sistemi protettivi antincendio Modalità di controllo dell'applicazione Sistemi intumescenti*. Febbraio 2001
- Norma Italiana UNI 10898-2-2003: *Sistemi protettivi antincendio Modalità di controllo dell'applicazione Sistemi in lastre*. Ottobre 2003
- Norma Italiana UNI 10898-3-2007: *Sistemi protettivi antincendio Modalità di controllo dell'applicazione Parte 3: Sistemi isolanti spruzzati (spray)*. Ottobre 2003
- Norma Europea UNI EN 1473-2007: *Installazioni ed equipaggiamenti per il gas naturale liquefatto (GNL) Progettazione delle installazioni di terra*. Marzo 2007
- Oven Manual

- Ptáček P., Kubátová D., Havlica J., Brandštetr J., Šoukal F., Opravil T.: *The non-isothermal kinetic analysis of the thermal decomposition of kaolinite by Thermogravimetric analysis*. August, 2010.
- Reynolds, R.A., Russell, G.W., and Nourse, R.W.: *Ablation Performance Characterization of Thermal Protection Materials Using a Mach 4.4 Sled Test*. AIAA/SAE/ASME/ASEE. July 1992.
- TGA Manual
- Tubular Furnace Manual
- Università di Pisa: Prometeo: Il portale della Ricerca dell'Università di Pisa. Web site: <http://prometeo.adm.unipi.it/attrezzature.php?set=4&dip=300026&ide=3035&l=0>
- Villain G., Thiery M., Platret G.: *Measurement methods of carbonation profiles in concrete: thermogravimetry, chemical analysis and gammadensimetry*. April, 2007.

APPENDIX A

Tests before oven drying:

| | Date mm/dd/yy | ID | Air/ Nitrogen | Material | Virgin/ burned | Fire exposure time (min) | Depth | Sample (mg) | Heating rate (°C/min) | Particle size | Procedure |
|----|------------------|-----------------------------------|---------------|-----------|----------------|--------------------------------|-------|----------------|-----------------------------|------------------|-----------------------------|
| 1 | 09/22/10 | NFenB15D19-10mg-10-001 | Nitrogen | Fendolite | Burned | 15 | 19mm | 12.95 | 10 | chunk | Test10Cmin |
| 2 | 09/27/10 | NFenV10mg-10Cmin850-001 | Nitrogen | Fendolite | Virgin | 0 | 0mm | 12 | 10 | chunk | Test10Cmin850C |
| 3 | 09/27/10 | NFenV10mg-10Cmin850-001residuo | Nitrogen | Fendolite | Virgin | 0 | 0mm | / | 10 | chunk | Test10Cmin850C |
| 4 | 09/27/10 | NFenV10mg-10Cmin850-002 | Nitrogen | Fendolite | Virgin | 0 | 0mm | 11.89 | 10 | chunk | Test10Cmin850C |
| 5 | 09/28/10 | NFenV10mg-10Cmin850-001rehydrated | Nitrogen | Fendolite | Virgin | 0 | 0mm | 9.6 | 10 | chunk | Test10Cmin850C |
| 6 | 09/29/10 | NFenB15D19-10mg-10-002 | Nitrogen | Fendolite | Burned | 15 | 19mm | 10.7 | 10 | chunk | Test10Cmin |
| 7 | 09/29/10 | NFenB15D0-10mg-10-001 | Nitrogen | Fendolite | Burned | 15 | 0mm | 11.6 | 10 | chunk | Test10Cmin |
| 8 | 09/30/10 | NFenB15D0-10mg-10-002 | Nitrogen | Fendolite | Burned | 15 | 0mm | 12 | 10 | chunk | Test10Cmin |
| 9 | 09/30/10 | NFenB50D0-10mg-10-001 | Nitrogen | Fendolite | Burned | 50 | 0mm | 11.7 | 10 | chunk | Test10Cmin |
| 10 | 10/01/10 | NFenB50D0-10mg-10-002 | Nitrogen | Fendolite | Burned | 50 | 0mm | 12 | 10 | chunk | Test10Cmin |
| 11 | 10/01/10 | NFenV10mg-10Cmin-001 | Nitrogen | Fendolite | Virgin | 0 | 0mm | 13 | 10 | chunk | Test10Cmin |
| 12 | 10/01/10 | NFenV10mg-10Cmin-001residue | Nitrogen | Fendolite | Virgin | 0 | 0mm | / | 10 | chunk | Test10Cmin |
| 13 | 10/05/10 | NFenB50D19-10mg-10-001 | Nitrogen | Fendolite | Burned | 50 | 19mm | 10 | 10 | chunk | Test10Cmin |
| 14 | 10/05/10 | NFenB50D19-10mg-10-002 | Nitrogen | Fendolite | Burned | 50 | 19mm | 14 | 10 | chunk | Test10Cmin |
| 15 | 10/06/10 | ONCHB10mg-10-001 | Nitrogen | Chartek7 | oven burned | / | / | 12.6 | 10 | chunk | Test10Cmin |
| 16 | 10/06/10 | ONCHB10mg-10-002 | Nitrogen | Chartek7 | oven burned | / | / | 10 | 10 | chunk | Test10Cmin |
| 17 | 10/06/10 | NCemV10mg-10-001 | Nitrogen | Cement | Virgin | 0 | 0mm | 11 | 10 | chunk | Test10Cmin |
| 18 | 10/08/10 | ONFenB10mg-10-001 | Nitrogen | Fendolite | oven burned | 0 | 0mm | 12 | 10 | chunk | Test10Cmin |
| 19 | 10/08/10 | NFenV10mg-10Cmin-001rehydrated | Nitrogen | Fendolite | Virgin | 0 | / | 16 | 10 | chunk | Test10Cmin |
| 20 | 10/11/10 | ONFenV10mg-10Cmin-002 | Nitrogen | Fendolite | oven burned | / | / | 9.8 | 10 | chunk | Test10Cmin |
| 21 | 10/12/10 | NFenV10mg-10Cmin400-001 | Nitrogen | Fendolite | Virgin | / | / | | 10 | chunk | Test10Cmin-400C-2h-isotherm |
| 22 | 10/13/10 | ONCHB10mg-10-003 | Nitrogen | Chartek7 | oven burned | / | / | | 10 | chunk | Test10Cmin |
| 23 | 10/14/10 | ONCHB10mg-10-004B | Nitrogen | Chartek7 | oven burned | / | / | 12.8 | 10 | chunk | Test10Cmin |
| 24 | 10/14/10 | ONCHB10mg-10-004NB | Nitrogen | Chartek7 | oven burned | / | / | 12 | 10 | chunk | Test10Cmin |
| 25 | 10/14/10 | NCHV10mg-10-004 | Nitrogen | Chartek7 | Virgin | / | / | 11.5 | 10 | chunk | Test10Cmin |
| 26 | 10/15/10 | NMic10mg-10-001 | Nitrogen | Mica | Virgin | / | / | 10.9 | 10 | sheets | Test10Cmin |
| 27 | 10/15/10 | NFenV10mgPow0045-10-001 | Nitrogen | Fendolite | Virgin | / | / | 12 | 10 | powder | Test10Cmin |

Characterization of the degradation behaviour of Passive Fire Protector Materials

| | | | | | | | | | | | |
|----|----------|--------------------------------|----------|-----------|-------------|---|-----|-------|----|--------|-------------------------|
| 28 | 10/18/10 | ONCHB10mg250C-10-005 | Nitrogen | Chartek7 | oven burned | / | / | | 10 | chunk | Test10Cmin |
| 29 | 10/18/10 | NCHV10mg-10-005 | Nitrogen | Chartek7 | Virgin | / | / | 12.59 | 10 | chunk | Test10Cmin |
| 30 | 10/18/10 | NFenV10mg1week-rehyd-10-001 | Nitrogen | Fendolite | Virgin | / | / | | 10 | chunk | Test10Cmin |
| 31 | 10/18/10 | NFenV10mg-5-001 | Nitrogen | Fendolite | Virgin | 0 | 0mm | | 5 | chunk | Test5Cmin |
| 32 | 10/19/10 | ONCHB10mg300C-10-006 | Nitrogen | Chartek7 | oven burned | / | / | 12.5 | 10 | chunk | Test10Cmin |
| 33 | 10/19/10 | NFenV10mg-5-002 | Nitrogen | Fendolite | Virgin | 0 | 0mm | 11.13 | 5 | chunk | Test5Cmin |
| 34 | 10/19/10 | NCHV10mg-10-006 | Nitrogen | Chartek7 | Virgin | / | / | 13.81 | 10 | chunk | Test10Cmin |
| 35 | 10/20/10 | ONCHB10mg400C-10-007 | Nitrogen | Chartek7 | oven burned | / | / | | 10 | chunk | Test10Cmin |
| 36 | 10/20/10 | NMic10mg-10-002 | Nitrogen | Mica | Virgin | / | / | | 10 | sheets | Test10Cmin900C-iso1min |
| 37 | 10/21/10 | ONCHB10mg400C-10-008sp1 | Nitrogen | Chartek7 | oven burned | / | / | | 10 | chunk | Test10Cmin |
| 38 | 10/21/10 | ONCHB10mg400C-10-008sp2 | Nitrogen | Chartek7 | oven burned | / | / | | 10 | chunk | Test10Cmin |
| 39 | 10/21/10 | ONCHB10mg400C-10-008sp3 | Nitrogen | Chartek7 | oven burned | / | / | | 10 | chunk | Test10Cmin |
| 40 | 10/21/10 | NCHV10mg400C-10-Iso2h-001 | Nitrogen | Chartek7 | Virgin | / | / | | 10 | chunk | Isotherm @ 400C 2 hours |
| 41 | 10/21/10 | NCHV10mg500C-10-Iso2h-001 | Nitrogen | Chartek7 | Virgin | / | / | | 10 | chunk | Isotherm @ 500C 2 hours |
| 42 | 10/25/10 | NFenV10mg-10iso30-001 | Nitrogen | Fendolite | Virgin | / | / | 12.67 | 10 | chunk | Iso30 |
| 43 | 10/25/10 | NFenV10mg-10iso50-001 | Nitrogen | Fendolite | Virgin | / | / | 10.2 | 10 | chunk | Iso50 |
| 44 | 10/26/10 | ONCHB10mg400C-10-009-0,5sp | Nitrogen | Chartek7 | oven burned | / | / | 10.59 | 10 | chunk | Test10Cmin |
| 45 | 10/26/10 | NFenV10mg-10iso50-002 | Nitrogen | Fendolite | Virgin | / | / | 12.44 | 10 | chunk | Iso50 |
| 46 | 10/27/10 | ONCHB10mg600C-10-010 | Nitrogen | Chartek7 | oven burned | / | / | 10.14 | 10 | chunk | Test10Cmin |
| 47 | 10/27/10 | NFenV30mg-10-001top | Nitrogen | Fendolite | Virgin | / | / | 30.78 | 10 | chunk | Test10Cmin950C |
| 48 | 10/27/10 | NFenV30mg-10-002bottom | Nitrogen | Fendolite | Virgin | / | / | | 10 | chunk | Test10Cmin950C |
| 49 | 10/28/10 | NMic10mg950C-10-003 | Nitrogen | Mica | Virgin | / | / | 10 | 10 | sheets | Test10Cmin950C |
| 50 | 10/28/10 | NFenV30mg-10-003estufa24h | Nitrogen | Fendolite | Virgin | / | / | 30 | 10 | chunk | Test10Cmin |
| 51 | 11/02/10 | NCHV10mg-jump500C-10-iso2h-001 | Nitrogen | Chartek7 | virgin | / | / | 10 | 10 | chunk | Testjump500C2h |
| 52 | 11/02/10 | NFenV30mg-10-003estufa6d | Nitrogen | Fendolite | Virgin | / | / | 30 | 10 | chunk | Test10Cmin |
| 53 | 11/02/10 | NCHV10mg-jump400C-10-iso2h-001 | Nitrogen | Chartek7 | virgin | / | / | 10 | 10 | chunk | Testjump400Ciso2h |
| 54 | 11/02/10 | NCHV10mg-jump600C-10-iso2h-001 | Nitrogen | Chartek7 | virgin | / | / | 10 | 10 | chunk | Testjump600Ciso2h |
| 55 | 11/03/10 | ONCHB10mg800C-10-011 | Nitrogen | Chartek7 | oven burned | / | / | 10.06 | 10 | chunk | Test10Cmin |
| 56 | 11/04/10 | ONCHB10mg600C-10-012 | Nitrogen | Chartek7 | oven burned | / | / | 12.5 | 10 | chunk | Test10Cmin |
| 57 | 11/04/10 | NFenV30mg-10-004-estufa110-1d | Nitrogen | Fendolite | Virgin | / | / | 30 | 10 | chunk | Test10Cmin |
| 58 | 11/04/10 | NFenV30mg-10-005-estufa110-1d | Nitrogen | Fendolite | Virgin | / | / | 30 | 10 | chunk | Test10Cmin |
| 59 | 11/05/10 | NFenV30mg-10-006-estufa110-2d | Nitrogen | Fendolite | Virgin | / | / | 30 | 10 | chunk | Test10Cmin_storageon |

APPENDIX B

Tests after oven drying:

| | Date mm/dd/yy | ID | Air/ Nitrogen | Material | Virgin/ burned | Sample weight (mg) | Heating rate (°C/min) | Particle size | Procedure |
|----|------------------|------------------------------|------------------|-----------|-------------------|--------------------------|-----------------------------|------------------|--|
| 1 | 11/8/2010 | NFenV30mg-10-001c | Nitrogen | Fendolite | heater 110C | ~30 | 10 | chunk | Test10Cmin-storageon |
| 2 | 11/8/2010 | NFenV30mg-10-002c | Nitrogen | Fendolite | heater 110C | ~30 | 10 | chunk | Test10Cmin-storageon |
| 3 | 11/8/2010 | NFenV30mg-25-001c | Nitrogen | Fendolite | heater 110C | ~30 | 25 | chunk | 25 |
| 4 | 11/9/2010 | NFenV30mg-25-002c | Nitrogen | Fendolite | heater 110C | ~30 | 25 | chunk | 25 |
| 5 | 11/9/2010 | ONFenV30mg250C-10-iso2h-001 | Nitrogen | Fendolite | oven burned | ~30 | 10 | chunk | Test10Cmin-storageon |
| 6 | 11/9/2010 | NFenV30mg-5-001c | Nitrogen | Fendolite | heater 110C | ~30 | 5 | chunk | Test5Cmin |
| 7 | 11/10/2010 | ONFenV30mg350C-10-iso2h-002 | Nitrogen | Fendolite | oven burned | ~30 | 10 | chunk | Test10Cmin-storageon |
| 8 | 11/10/2010 | NFenV30mg950C-25-003c | Nitrogen | Fendolite | heater 110C | ~30 | 25 | chunk | 25 til 950C, no air change, iso 10min |
| 9 | 11/10/2010 | NFenV30mg-5-002c | Nitrogen | Fendolite | heater 110C | ~30 | 5 | chunk | Test5Cmin |
| 10 | 11/11/2010 | NFenV30mg950C-45-001c | Nitrogen | Fendolite | heater 110C | ~30 | 45 | chunk | Test45Cmin950C |
| 11 | 11/11/2010 | ONFenV30mg500C-10-iso2h-003 | Nitrogen | Fendolite | oven burned | ~30 | 10 | chunk | Test10Cmin-storageon |
| 12 | 11/12/2010 | NFenV30mg950C-45-002c | Nitrogen | Fendolite | heater 110C | ~30 | 45 | chunk | Test45Cmin950C |
| 13 | 11/12/2010 | ONFenV30mg800C-10-iso2h-004 | Nitrogen | Fendolite | oven burned | 25 | 10 | chunk | iso2h |
| 14 | 11/15/2010 | NFenV30mg950C-25-004c | Nitrogen | Fendolite | heater 110C | ~40 | 25 | chunk | 25til950C |
| 15 | 11/16/2010 | NFenV30mg-10-003c | Nitrogen | Fendolite | heater 110C | ~30 | 5 | chunk | Test10Cmin-storageon |
| 16 | 11/16/2010 | NFenV30mg-5-003c | Nitrogen | Fendolite | heater 110C | ~30 | 5 | chunk | Test5Cmin |
| 17 | 11/17/2010 | NFenV30mg950-45-003c | Nitrogen | Fendolite | heater 110C | ~30 | 45 | chunk | Test45Cmin950C |
| 18 | 11/18/2010 | ONFenV30mg350C-10-iso2h-002b | Nitrogen | Fendolite | oven burned | ~30 | 10 | chunk | Test10Cmin-storageon |
| 19 | 11/19/2010 | ONFenV30mg500C-10-iso2h-003b | Nitrogen | Fendolite | oven burned | ~30 | 10 | chunk | Test10Cmin-storageon |
| 20 | 11/23/2010 | NFenV30mg-10-500Ciso2h-001 | Nitrogen | Fendolite | heater 110C | ~30 | 10 | chunk | 500Ciso2h |
| 21 | 11/23/2010 | NFenV30mg-10-350Ciso2h-001 | Nitrogen | Fendolite | heater 110C | ~30 | 10 | chunk | 350Ciso2h |
| 22 | 11/23/2010 | NCHV10mg-jump-350Ciso2h-001 | Nitrogen | Fendolite | Virgin | ~30 | / | chunk | 350Ciso2h |
| 23 | 11/23/2010 | NCHV10mg-jump-450Ciso2h-001 | Nitrogen | Fendolite | Virgin | ~30 | / | chunk | 450Ciso2h |
| 24 | 11/24/2010 | ONCHB10mg250C-10-013 | Nitrogen | Chartek | oven burned | 12 | 10 | chunk | Test10Cmin-storageon |
| 25 | 11/24/2010 | NFenV30mg-10-250Ciso2h-001 | Nitrogen | Fendolite | heater 110C | ~30 | 10 | chunk | 250Ciso2h |

Characterization of the degradation behaviour of Passive Fire Protector Materials

| | | | | | | | | | |
|----|------------|--------------------------------------|----------|-----------|-------------|------|----|--------|----------------------|
| 26 | 11/25/2010 | ONCHB10mg200C-10-014 | Nitrogen | Chartek | oven burned | 12 | 10 | chunk | Test10Cmin-storageon |
| 27 | 11/25/2010 | NCHV10mg-45-004 | Nitrogen | Fendolite | Virgin | ~30 | 45 | chunk | Test45Cmin950C |
| 28 | 11/25/2010 | NCHV10mg-10-007 | Nitrogen | Fendolite | Virgin | 10 | 10 | chunk | Test10Cmin-storageon |
| 29 | 11/29/2010 | ONCHB10mg350C-10-015 | Nitrogen | Chartek | oven burned | 12 | 10 | chunk | Test10Cmin-storageon |
| 30 | 12/9/2010 | ONCHB10mg325C-10-016 | Nitrogen | Chartek | oven burned | ~10 | 10 | chunk | Test10Cmin-storageon |
| 31 | 12/10/2010 | ONCHB10mg375C-10-017 | Nitrogen | Chartek | oven burned | 11,6 | 10 | chunk | Test10Cmin-storageon |
| 32 | 12/10/2010 | ONCHB10mg375C-10-018 | Nitrogen | Chartek | oven burned | 13 | 10 | chunk | Test10Cmin-storageon |
| 33 | 12/13/2010 | ONCHB10mg375C-10-019 | Nitrogen | Chartek | oven burned | ~10 | 10 | chunk | Test10Cmin-storageon |
| 34 | 12/15/2010 | ONCHB10mg325C-10-020 | Nitrogen | Chartek | oven burned | ~11 | 10 | chunk | Test10Cmin-storageon |
| 35 | 12/17/2010 | NFenV10mg-10Cmin-powder-001 | Nitrogen | Fendolite | heater 110C | ~10 | 10 | powder | Test10Cmin-storageon |
| 36 | 12/17/2010 | NFenV10mg-powder-10-002 | Nitrogen | Fendolite | heater 110C | ~10 | 10 | powder | Test10Cmin-storageon |
| 37 | 1/12/2011 | NfenV30mg-5-powder-001 | Nitrogen | Fendolite | heater 110C | ~30 | 5 | powder | Test5Cmin |
| 38 | 1/13/2011 | NfenV30mg-5doublegas-powder-002 | Nitrogen | Fendolite | heater 110C | ~30 | 5 | powder | Test5Cmin |
| 39 | 1/13/2011 | NfenV30mg-5doublegas-003 | Nitrogen | Fendolite | heater 110C | ~30 | 5 | chunk | Test5Cmin |
| 40 | 1/17/2011 | NfenV30mg-5-004 | Nitrogen | Fendolite | heater 110C | ~30 | 5 | chunk | Test5Cmin |
| 41 | 1/24/2011 | NfenV30mg950C-25-005doublegas | Nitrogen | Fendolite | heater 110C | ~30 | 25 | chunk | 25til950C |
| 42 | 1/24/2011 | NfenV30mg950C-25-005doublegas-powder | Nitrogen | Fendolite | heater 110C | ~30 | 25 | powder | 25til950C |
| 43 | 1/24/2011 | NfenV30mg950C-25-006 | Nitrogen | Fendolite | heater 110C | ~30 | 25 | chunk | 25til950C |
| 44 | 1/26/2011 | NfenV30mg-10-004 | Nitrogen | Fendolite | heater 110C | ~30 | 10 | chunk | Test10Cmin |

